How C–C Bonds Are Formed and How They Influence Structural Choices in Some Binary and Ternary Metal Carbides

Jing Li and Roald Hoffmann*

Department of Chemistry and Materials Science Center, Cornell University, Ithaca, New York 14853-1301

Received August 8, 1988

The dimeric C_2 unit has been found in many binary and ternary metal carbide systems. The C–C bond length in these crystal compounds varies over a wide range, from a conventional carbon–carbon single bond to a typical C–C triple bond. The formation of C_2 units is an important factor affecting the structural stability as well as other physical properties. In the UC_2 structure, both uranium–carbon bonding and carbon–carbon bonding are enhanced upon formation of such dimeric units and the system is greatly stabilized. Our calculations indicate that UC_2 is metallic, whereas the alkaline-earth metal carbide CaC_2, a structure belonging to the same crystal family, has a substantial gap between the valence and conduction bands. The pairing of carbon atoms in $DyCoC_2$ structure derives from a Peierls-type distortion. This crystal form should be favorable for electron counts of 19 → 21, with late transition-metal elements. Early transition-metal carbides of the same composition do not exist in this form and a rationale is given for this. $UCoC_2$, another stable form of RTC_2, also contains short C–C bonds. Structurally and electronically, comparisons are made of this structure and a closely related $UCuAs_2$ type, in which carbon atoms do not form bonds. It is found that the $UCoC_2$ structure is favorable for a valence electron count of 23 or less, whereas the $UCuAs_2$ form becomes more stable for 24 electrons or more. Finally, we discuss briefly two possible carbide forms of the $ThCr_2Si_2$ type structure.

Binary metal carbides have long been known to exist. Structures of this type are composed of two elements: carbon and the metal R, T, or A, where R designates by convention a rare-earth metal, T, a transition metal, and A, an alkaline-earth metal. One way of classifying the binary metal carbides is to group them by the extent of C–C bonding: those with short carbon–carbon contact in one class and the rest in the other. The CaC_2[1] (or UC_2[2]), ThC_2,[3] and Pu_2C_3[4] type structures shown in 1 belong to the first class. CaC_2 crystallizes in the body-centered tetragonal and ThC_2, in the monoclinic system at room temperature. Only a portion of the unit cell is shown for the body-centered cubic Pu_2C_3, to emphasize the local environment of the C_2 dimeric unit. A common feature of these three structure types is that there are distinct, strongly bondded C_2 pairs isolated from each other in the structures. The short contact between C_2 dimer and metal atoms also gives rise to strong metal–carbon interactions. Many members of this family exhibit interesting electric and magnetic properties. For example, all of the RC_2 compounds are intrinsically metallic, whereas the isostructural alkaline-earth metal carbides are insulators.[5-7] Most of these carbides have one or more high-temperature forms,[8-10] and a number of them become ferromagnetic or antiferromagnetic at low temperature.[1,6,11-16]

Table I. C–C Distances in Some Selected Binary and Ternary Metal Carbides

cryst struct	C–C, Å	ref
	Binary Carbides	
CaC_2	1.191, 1.20	1, 2
CeC_2	1.281, 1.283	1, 6
PrC_2	1.294	6
NdC_2	1.291	6
TbC_2	1.291	6
HoC_2	1.279	6
LaC_2	1.280, 1.303	1, 5
ErC_2	1.288	13
SmC_2	1.285	1
TbC_2	1.293	1, 54
EuC_2	1.285	1
YbC_2	1.287	1, 54
GdC_2	1.285	1
YC_2	1.275	1, 2
LuC_2	1.276	1, 2
UC_2	1.34, 1.35	1, 2, 55, 56
ThC_2	1.47	3
ThC_2 (HT)	1.32	8
Pu_2C_3	1.54	4
Pr_2C_3	1.239	57
La_2C_3	1.236, 1.32	5, 57
Ce_2C_3	1.276	6, 57
Tb_2C_3	1.240	57
Ho_2C_3	1.240 (5 K)	58
U_2C_3	1.295, 1.42	
	Ternary Carbides	
$UCoC_2$	1.48	19
$ScCoC_2$	1.26	23
$DyCoC_2$	1.37	24
$DyNiC_2$	1.37	24
$CeCoC_2$	1.36	30
U_2NiC_3	1.43	32
$Er_8Rh_5C_{12}$	1.27, 1.32	33
$La_2Ni_5C_3$	1.42	21
Er_2FeC_4	1.33	18

Ternary metal carbon compounds are also receiving increased attention, due to their potential importance in

(1) Atoji, M. *J. Chem. Phys.* **1961**, *35*, 1950. The paramagnetic scattering analysis revealed that U atom in UC_2 is possibly tetravalent.
(2) Atoji, M.; Medrud, R. *J. Chem. Phys.* **1959**, *31*, 332.
(3) Hunt, E. *J. Am. Chem. Soc.* **1951**, *73*, 4777.
(4) Zachariasen, W. H. *Acta Crystallogr.* **1952**, *5*, 17.
(5) Atoji, M.; Gschneider, Jr., K.; Daane, A. H.; Rundle, R. E.; Spedding, F. H. *J. Am. Chem. Soc.* **1958**, *80*, 1804.
(6) Atoji, M. *J. Chem. Phys.* **1967**, *46*, 1891.
(7) Stackelberg, M. V. *Z. Elektrochem.* **1931**, *37*, 542.
(8) Bowman, A. L.; Krikorian, N. H.; Arnold, G. P.; Wallace, T. C.; Nereson, N. G. *Acta Crystallogr.* **1968**, *B24*, 1121.
(9) Adachi, G.-Y.; Shibata, Y.; Ueno, K.; Shiokawa, J. *J. Inorg. Nucl. Chem.* **1976**, *38*, 1023.
(10) Wells, A. F. *Structural Inorganic Chemistry*; 4th ed.; Clarendon Press: Oxford, 1975.
(11) Atoji, M. *J. Chem. Phys.* **1971**, *54*, 3504.
(12) Atoji, M.; Jsunoda, Y. *J. Chem. Phys.* **1971**, *54*, 3510.
(13) Atoji, M. *J. Chem. Phys.* **1972**, *57*, 2410.
(14) (a) Atoji, M. *J. Chem. Phys.* **1968**, *48*, 3384. (b) Atoji, M. *Ibid.* **1970**, *52*, 6430, 6431.

0897-4756/89/2801-0083$01.50/0

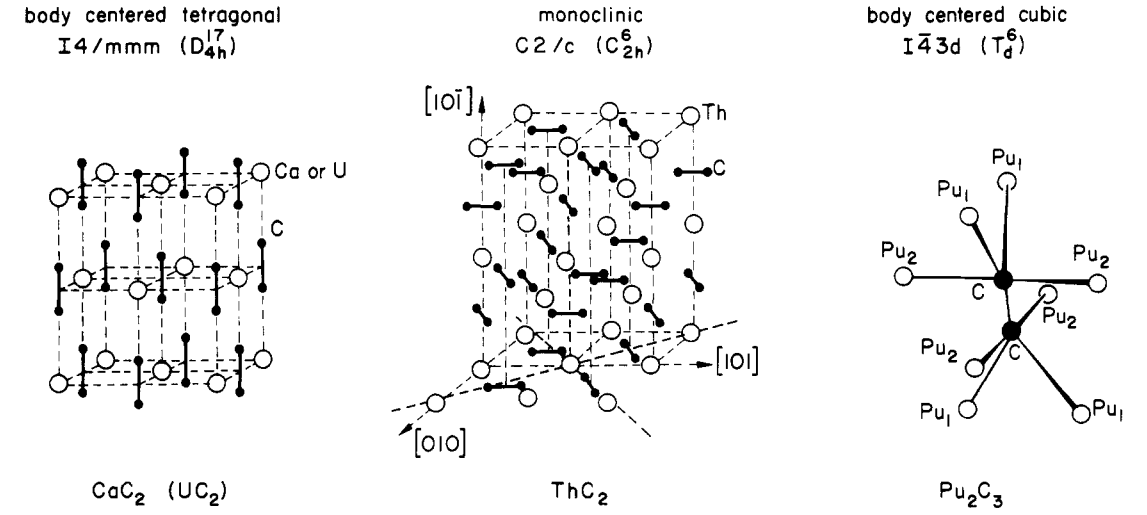

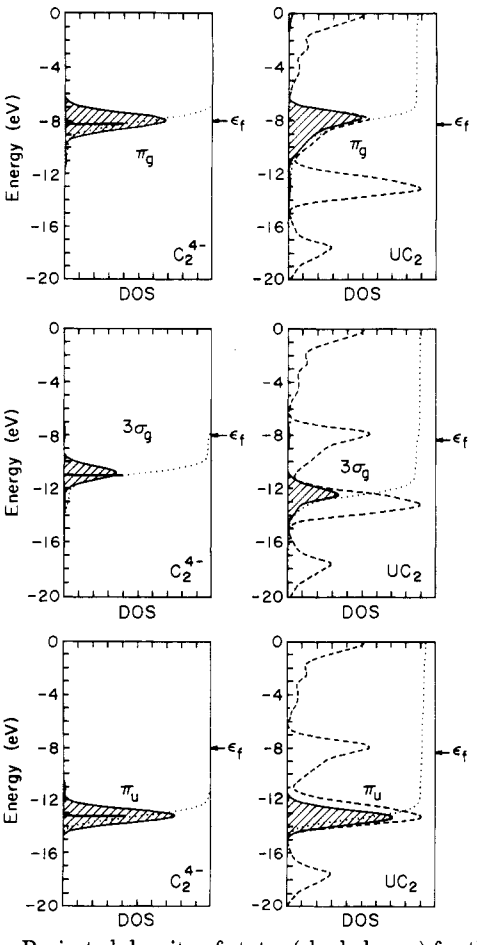

Figure 1. Projected density of states (shaded area) for the UC_2 structure. At left are the DOS of π_g, $3\sigma_g$, and π_u in a three-dimensional C_2^{4-} lattice, and at right the corresponding projections in UC_2. Sticks in the left panels indicate orbital energies of molecular C_2. Dotted lines give integrations of the projected orbitals, and dashed lines are the total DOS. Fermi energy is indicated by an arrow.

nuclear technology and in making permanent magnets. Numerous investigations on conductivity and magnetic properties have been made on $R_2Fe_{14}C$ systems (R = Gd, Dy, Er, Lu).[17] It has been reported that Er_2FeC_4 is paramagnetic at room temperature and Y_2FeC_4 becomes superconducting at T_c = 3.6 K.[18] Like the binary systems, the ternary carbides can be classified into two categories: (1) structures containing bonded carbon pairs[18-33] and (2) those with isolated C atoms.[34-53] Illustrated in **2** are two

(15) Atoji, M. *J. Solid State Chem.* **1978**, *26*, 51.
(16) Atoji, M. *J. Chem. Phys.* **1967**, *46*, 4148.
(17) (a) Stadelmaier, H. H.; Park, H. K. *Z. Metallkd.* **1981**, 417. (b) Abache, C.; Oesterreicher, H. *J. Appl. Phys.* **1985**, *57*, 4112. (c) Pedziwiatr, A. T.; Wallace, W. E.; Burzo, E. *J. Magn. Magn. Mater.* **1986**, *59*, L179. (d) Liu, N. C.; Stadelmaier, H. H. *Mater. Lett.* **1986**, *4*, 377. (e) Liu, N. C.; Stadelmaier, H. H.; Schneider, G. *J. Appl. Phys.* **1987**, *61*, 3574. (f) Denissen, C. J. M.; de Mooij, B. D.; Buschow, K. H. J. *J. Less-Common Met.* **1988**, *139*, 291.
(18) Gerss, M. H.; Jeitschko, W.; Boonk, L.; Nientiedt, J.; Grobe, J.; Mörsen, E.; Leson, A. *J. Solid State Chem.* **1987**, *70*, 19.
(19) Gerss, M. H.; Jeitschko, W. *Mater. Res. Bull.* **1986**, *21*, 209.
(20) Tsokol', A. O.; Bodak, O. I.; Marusin, E. P. *Sov. Phys. Crystallogr.* **1986**, *31*, 466.
(21) Tsokol', A. O.; Bodak, O. I.; Marusin, E. P. *Sov. Phys. Crystallogr.* **1986**, *31*, 39.
(22) Arai, Y.; Suzuki, Y.; Sasayama, T.; Watanabe, H. *J. Nucl. Sci. Technol.* **1982**, *19*, 257.
(23) Marusin, E. P.; Bodak, O. I.; Tsokol', A. O.; Baivel'man, M. G. *Sov. Phys. Crystallogr.* **1985**, *30*, 340.
(24) Jeitschko, W.; Gerss, M. H. *J. Less-Common Met.* **1986**, *116*, 147.
(25) Semenenko, K. N.; Putyatin, A. A.; Nikol'skaya, I. V.; Burnasheva, V. V. *Russ. J. Inorg. Chem.* **1983**, *28*, 943.
(26) Bodak, O. I.; Marusin, E. P. *Dokl. Akad. Nauk Ukr. S.S.R. Ser. A* **1979**, *12*, 1048.
(27) Gerss, M. H. Diplomarbeit, Universität Dortmund, July, 1983.
(28) Gerss, M. H.; Jeitschko, W. *Abstr. 8th Eur. Crystallogr. Meet.*, Liêge, Aug 8-12, 1983; p 106.
(29) Gerss, M. H.; Jeitschko, W. *4 Vortragstagg. Gesellsch. dt. Chem. Fachgr. Festkörperchem*, Aachen, Aug 20-22, 1984.
(30) Bodak, O. I.; Marusin, E. P.; Bruskov, V. A. *Sov. Phys. Crystallogr.* **1980**, *25*, 355.
(31) Stadelmaier, H. H.; Liu, N.-C. *Z. Metallkd.* **1985**, *76*, 585.
(32) Gerss, M. H.; Jeitschko, W. *Z. Kristallogr.* **1986**, *175*, 203.
(33) Hoffmann, R.-D.; Jeitschko, W. *Z. Kristallogr.* **1986**, *174*, 85.
(34) Spear, K. E.; Leitnaker, J. M.; Lindemer, T. B. *High Temp. Sci.* **1970**, *2*, 176.
(35) Jeitschko, W.; Behrens, R. K. *Z. Metallkde.* **1986**, *12*, 788.
(36) Nowotny, H.; Kieffer, R.; Benesovsky, F.; Laube, E. *Monatsh. Chem.* **1958**, *89*, 692.
(37) Rudy, E.; Benesovsky, F. *Monatsch. Chem.* **1963**, *94*, 85.
(38) Cromer, D. T.; Larson, A. C.; Roof, Jr., R. B. *Acta Crystallogr.* **1964**, *17*, 272.
(39) Farr, J. D.; Bowman, M. G. *Carbides in Nuclear Energy*; Russell, L. E., Ed.; Macmillan, London, 1964; pp 184-191.
(40) Alekseyeva, Z. M.; Ivanov, O. S. *Proc. 4th Symp. Thermodyn. Nucl. Mater.* **1975**, *2*, 175.
(41) Ugajin, M.; Suzuki, Y.; Shimokawa, J. *J. Nucl. Mater.* **1972**, *43*, 277.
(42) Haines, H. R.; Mardon, P. G.; Potter, P. E. *Plutonium and Other Actinides*; Bland, H., Linder, R., Eds.; NorthHolland: Amsterdam, 1976; pp 233-244.

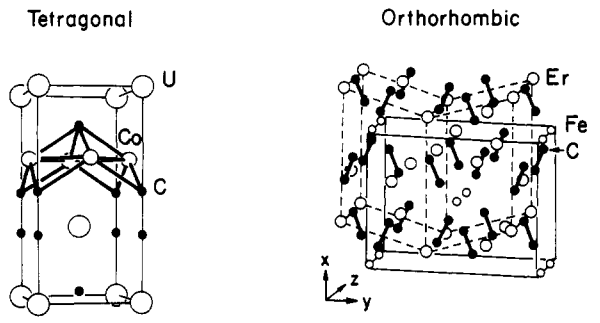

2

examples of group 1 materials: the tetragonal $UCoC_2$ and the orthorhombic Er_2FeC_4. The carbon atoms form dimers in each structure. In addition, there are short transition metal–metal bonds in these structures, i.e., Co–Co = 2.47 Å in $UCoC_2$ and Fe–Fe = 2.50 Å in Er_2FeC_4.

For both binary and ternary metal carbides, the C–C distances found in compounds of the first category vary over a wide range, for instance, from 1.19 Å in CaC_2[1] and 1.26 Å in $ScCoC_2$[23] to 1.37 and 1.54 Å in $DyCoC_2$[24] and Pu_2C_3.[4] Some selected examples are listed in Table I. Compounds of the second category do not possess any short carbon–carbon bonds. Examples of these include $UMoC_2$,[35] YCoC,[48] and UC,[55] in which C–C distances are 2.87, 3.65, and 3.50 Å, respectively. A great number of crystal structures of this kind are metal rich, such as the binary Fe_3C[60] and Cr_7C_3[61] and ternary $R_2Ni_{22}C_3$ (R = Ce, La, Pr)[46] and $La_2Fe_{14}C$.[47]

In addition to the metal carbides described above, there is another series of cluster type ternary carbides that contain not only metal and carbon atoms but also group VIIA elements, Cl, Br, and I.[62-65] The carbon atoms in these compounds also form pairs. Electronic structure calculations have been performed on $Gd_{10}Cl_{18}C_4$,[66,67] $Gd_{10}Cl_{17}C_4$, $Gd_{12}I_{17}C_6$,[67] and $Gd_2C_2Cl_2$[68] of this type. For the first three compounds, which contain short metal–metal contacts, the emphasis has been on the extent of metal–metal bonding.

Why do carbon atoms form pairs in some materials but not in others? How does the C–C bonding affect the stability of a crystal structure? By exploring the electronic properties of a variety of carbide systems, we wish to understand the role of carbon–carbon bond formation and the extent of such bonding. By the same token, we also hope to gain some insight into structural relationships of various metal carbides to related systems, so as to provide some guidelines for synthesizing new metal carbides. The systems we will examine include binary UC_2 (CaC_2) and ternary $DyCoC_2$ and $UCoC_2$ ($ScCoC_2$). The extended Hückel[69] tight-binding[70] approach serves as a handy computational tool. Detailed information on geometric data and atomic parameters used in the studies can be obtained from the Appendix.

Orbitals of Diatomic C_2

Crucial to our discussion will be the C_2 unit, sometimes fully formed, sometimes not, in these solid-state structures. The electronic structure of this diatomic is, of course, very well-known. The orbitals of a typical homonuclear diatomic are shown in **3**. In C_2 the $3\sigma_g$ (lone-pair combination) and π_u (strongly bonding) orbitals are close to each other in energy. The ground state of C_2 has the configuration $(1\sigma_g)^2(1\sigma_u)^2(2\sigma_g)^2(2\sigma_u)^2(1\pi_u)^4$, $^1\Sigma_g^+$.[71] The equilibrium bond length is 1.31 Å. A number of excited states are well characterized. These have distances between 1.23 and 1.53 Å, thus spanning just about the range of C–C distances in organic molecules and also those in the carbides under consideration.

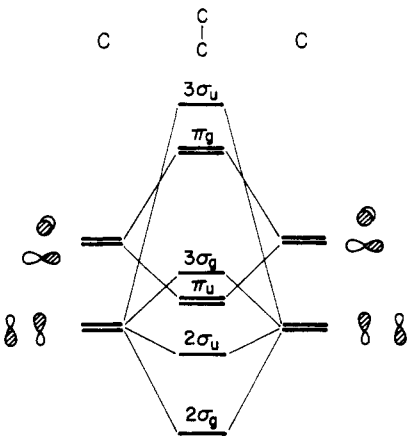

3

C_2^{2-} (14 electrons, 10 valence electrons) would be isoelectronic to nitrogen and should have a shorter equilibrium distance corresponding to the configuration $(1\sigma_g)^2(1\sigma_u)^2(2\sigma_g)^2(2\sigma_u)^2(1\pi_u)^4(3\sigma_g)^2$. C_2^{4-} would be isoelectronic with O_2, and C_2^{6-} with F_2, so the distances should increase with reduction of the C_2 unit. Throughout this paper we will refer not to the total number of electrons in the C_2 unit but to the valence electrons only, i.e., 8 in neutral C_2, 12 in C_2^{4-}, etc.

(43) Chubb, W.; Keller, D. L. *Carbides in Nuclear Energy*; Russell, L. E., Ed.; Macmillan: London, 1964; pp 208–229.
(44) Dalton, J. T.; Potter, P. E.; Shaw, J. L. *Plutonium*; Chapman and Hall: London, 1965; pp 775–805.
(45) Holleck, H. J. *Nucl. Mater.* **1984**, *124*, 129.
(46) Bodak, O. I.; Marusin, E. P.; Fundamenskii, V. S.; Bruskov, V. A. *Sov. Phys. Crystallogr.* **1982**, *27*, 657.
(47) Marusin, E. P.; Bodak, O. I.; Tsokol', A. O.; Fundamenskii, V. S. *Sov. Phys. Crystallogr.* **1985**, *30*, 338.
(48) Gerss, M. H.; Jeitschko, W. *Z. Naturforsch.* **1986**, *41B*, 946.
(49) Behrens, R. K.; Jeitschko, W. *Z. Kristallogr.* **1986**, *174*, 11.
(50) Holleck, H. *J. Nucl. Mater.* **1972**, *42*, 278.
(51) Block, G.; Jeitschko, W. *Inorg. Chem.* **1986**, *25*, 279.
(52) Jeitschko, W.; Block, G. *Z. Anorg. Allg. Chem.* **1985**, *528*, 61.
(53) Block, G.; Jeitschko, W. *Z. Kristallogr.* **1986**, *174*, 19.
(54) Gebelt, R. E.; Eick, H. A. *Inorg. Chem.* **1964**, *3*, 335.
(55) Austin, A. E. *Acta Crystallogr.* **1959**, *12*, 159.
(56) Atoji, M. *J. Chem. Phys.* **1967**, *47*, 1188.
(57) Atoji, M.; Williams, D. E. *J. Chem. Phys.* **1961**, *35*, 1960.
(58) Atoji, M.; Tsunoda, Y. *J. Chem. Phys.* **1971**, *54*, 3510.
(59) Novion, C. De.; Krebs, J. P.; Meriel, P. *Compt. Rend.* **1966**, *263B*, 457.
(60) Aronson, B.; Rundqvist, S. *Acta Crystallogr.* **1962**, *15*, 878.
(61) Fasiska, E. J.; Jeffrey, G. A. *Acta Crystallogr.* **1965**, *19*, 463.
(62) Simon, A.; Warkentin, E.; Masse, R. *Angew. Chem., Int. Ed. Engl.* **1981**, *20*, 1013.
(63) Warkentin, E.; Masse, R.; Simon, A. *Z. Anorg. Allg. Chem.* **1982**, *491*, 323.
(64) Simon, A.; Warkentin, E. *Z. Anorg. Allg. Chem.* **1983**, *497*, 79.
(65) Schwanitz-Schüller, U.; Simon, A. *Z. Naturforsch.* **1985**, *40B*, 710.
(66) Satpathy, S.; Anderson, O. K. *Inorg. Chem.* **1985**, *24*, 2604.
(67) Bullett, D. W. *Inorg. Chem.* **1985**, *24*, 3319.
(68) Miller, G. J.; Burdett, J. K.; Schwarz, C.; Simon, A. *Inorg. Chem.* **1986**, *25*, 4437.
(69) (a) Hoffmann, R. *J. Chem. Phys.* **1963**, *39*, 1397. (b) Hoffmann, R. *Lipscomb*, W. N. *Ibid.* **1962**, *37*, 2872. (c) Ammeter, J. H.; Burgi, H.-B.; Thibeault, J. C.; Hoffmann, R. *J. Am. Chem. Soc.* **1978**, *100*, 3686.
(70) Whangbo, M.-H.; Hoffmann, R. *J. Am. Chem. Soc.* **1978**, *100*, 6093.
(71) (a) Herzberg, G. *Spectra of Diatomic Molecules*; 1950, Van Nostrand Reinhold: 1950; pp 343, 513. (b) Another electron configuration for the ground state of C_2 is $(1\sigma_g)^2(1\sigma_u)^2(2\sigma_g)^2(2\sigma_u)^2(1\pi_u)^3(3\sigma_g)^1$, $^3\Pi_u$.

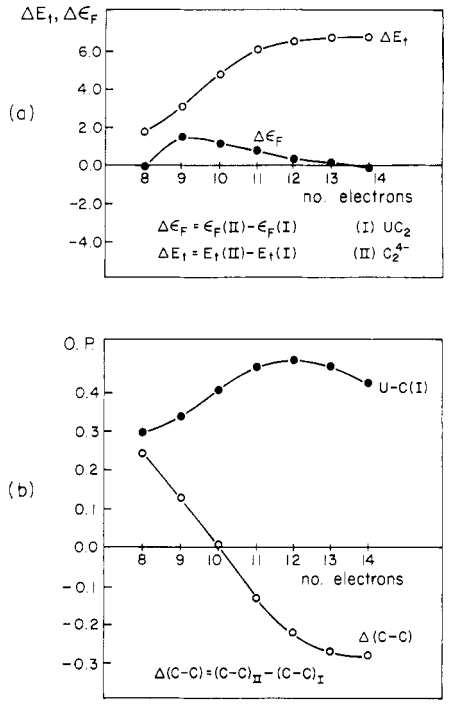

Figure 2. (a) Average total energy difference and Fermi energy difference between C_2^{4-} sublattice and the full UC_2 structure versus several electron counts. (b) Overlap population of U–C bond in UC_2 and change in overlap populations of the C–C bond in the two lattices.

UC_2 (CaC_2) Structure

As mentioned previously, the UC_2 type metal carbides contain discrete C_2 units. The molecular axis of C_2 orients parallel to the z direction of the cell, and the shortest C_2–C_2 separation is 3.52 Å. The C–C distance within a C_2 unit is 1.34 Å, a typical carbon–carbon double bond length were it found in a molecule. Formally, one could assign UC_2 as $U^{4+}(C_2)^{4-}$, i.e., uranium as a four-electron donor.[1] For an isolated C_2 species, this would half fill the π_g orbitals of C_2, indeed resulting in a double bond. What happens in the crystal? Let us consider first a sublattice of C_2^{4-}. Little interaction between dimeric units is expected since they are so far apart. This is reflected in the projected density of states shown at left of Figure 1 The sticks mark the energy values of π_u, $3\sigma_g$, and π_g orbitals of a single C_2 molecule. Notice that they reside in the central portion of the corresponding orbital projections in the solid, and the band width of each DOS is relatively narrow.

What if uranium atoms are added to the C_2 sublattice? The shortest U–C contact is 2.32 Å, a distance that is well within in the uranium–carbon bonding range. The uranium–carbon interactions are indeed quite strong, giving an overlap population of 0.487. The schematic diagram in **4** describes the interactions observed. Both $3\sigma_g$ and π_g states of C_2 are pushed down by U 6d orbitals. The 6d(U)–$\pi_u(C_2)$ interaction is comparably small, due to the large energy difference of the two, so that the majority of π_u states remain unchanged. Thus, energetically the system is stabilized by U atoms. Comparisons are made in Figure 2 between I, the UC_2 structure, and II, the C_2^{4-} sublattice. Figure 2a plots the energy differences of ϵ_F and E_t (Fermi energy and average total energy per unit cell) for the two systems as a function of valence electron count. The positive increasing $\Delta E_t = E_t(II) - E_t(I)$ implies continuous stabilization of I over II in the range of 8–14 electrons. $\Delta\epsilon_F = \epsilon_F(II) - \epsilon_F(I)$ shows a similar trend but not exactly the same: it is positive over an electron count of 9–13 and reaches its highest value at 9. For electron counts of 8 and

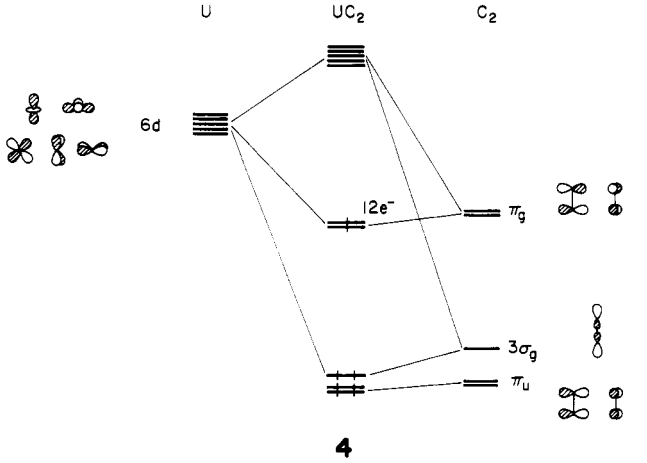

4

14, however, it is a little below the zero point.

Changes of overlap populations are traced in Figure 2b. It is interesting to observe that the change in the carbon–carbon overlap population, Δ(C–C), descends continuously between 8 and 14 electrons. This can be understood from the DOS projections in Figure 1. The C_2 orbitals that most strongly affect the C–C bond are certainly π_u and π_g for the electron counts considered. The $3\sigma_g$ orbital is a nonbonding type, so it is not very important for this context. The more the π_u is filled, or the less the π_g is occupied, the stronger the carbon–carbon bonding and the shorter the C–C bond. For lower electron counts, electrons fill the π_u states. Comparing the orbital projections of C_2^{4-} at left and those of UC_2 at right in Figure 1, one finds that part of π_u becomes unfilled in UC_2, due to its partial contribution to $\pi_u(C_2)$–6d(U) antibonding levels high up in energy. Therefore, with same number of electrons, the C–C bonding is stronger for C_2^{4-} than for UC_2 and Δ(C–C) is positive. However, as one adds more electrons to the system, the π_g states begin to be filled, and the situation reverses: for the same electron counts, π_g is now less occupied in UC_2 due to the $\pi_g(C_2)$–6d(U) interaction, giving rise to less antibonding between the two carbon atoms. The consequence of this is a decrease in Δ(C–C). For a 12-electron count, such as that we assign in $U^{4+}(C_2)^{4-}$, ~90% of π_u and ~40% of π_g are filled, and one again obtains a doubly bonded C_2. That the 12-electron assignment is reasonable can also be seen from the U–C overlap population curve plotted in Figure 2. A maximum is reached for a 12-electron count, the case of best bonding between the two atoms.

Now that we have understood how uranium atoms stabilize the crystal system of C_2^{4-}, we wish to proceed a little further, to see how the extent of C–C bonding varies with different electron counts. Obviously, when two neutral carbon atoms in the gas phase are brought together, they pair up. In other words, they form a bond because bonding molecular orbitals are stabilized (cf **3**). But suppose we add more and more electrons to the system. We will start to fill the antibonding MOs, which destabilize the C_2 moiety. Eventually, at an electron count of 16, for which the dimer is no longer stable, the C–C bond is completely destroyed. Does one find an analogy to this in the solid? The answer is a definite yes. What is plotted in Figure 3a are the energy differences between a system with C_2 units, symbolized as A, and one with isolated C atoms, B. Calculations have been performed on both UC_2 and CaC_2. In case A, the C–C interatomic distances are 1.34 and 1.19 Å in UC_2 and CaC_2, respectively, and for B, they are 2.34 Å in UC_2 and 2.38 Å in CaC_2. A is favored over B for lower electron counts, up to 13 with the UC_2 structure. For CaC_2,

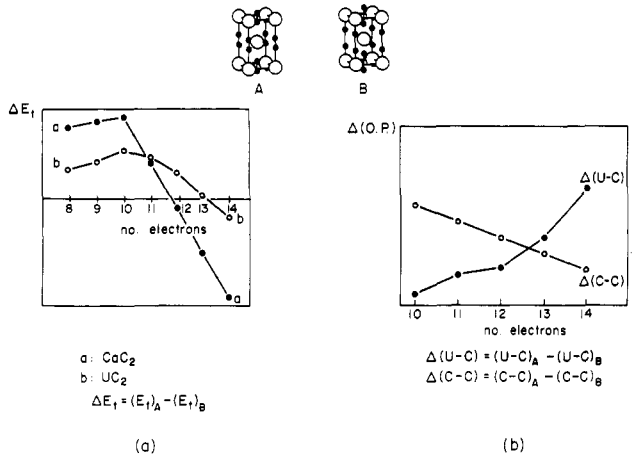

Figure 3. (a) Total energy change $\Delta E_t = E_t(B) - E_t(A)$ as a function of number of valence electrons in the systems. Configuration A is the UC_2 structure, whereas B does not contain a short C–C bond. Curve a is obtained for CaC_2 and curve b for UC_2. (b) Change in overlap populations for both U–C and C–C bonds in UC_2. The difference between configuration A and B is plotted.

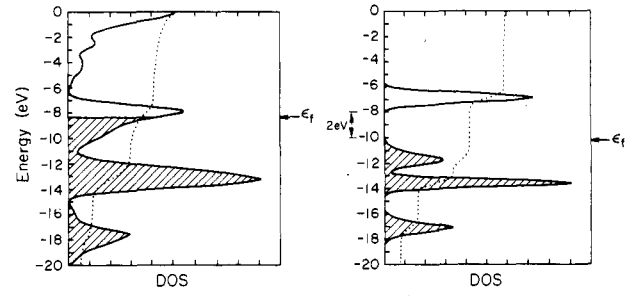

Figure 4. Total DOS projections for UC_2 at left and CaC_2 at right. The shaded area is filled with electrons. Fermi energy is indicated with an arrow. Dotted line is the integration of the total density of state.

11 is the turning point. For higher electron counts, B is more stable. A comparison of overlap populations of both the C–C and U–C bond in UC_2 is given in Figure 3b as $\Delta(U\text{–}C) = (U\text{–}C)_A - (U\text{–}C)_B$ and $\Delta(C\text{–}C) = (C\text{–}C)_A - (C\text{–}C)_B$. Positive values are obtained for the entire electron range considered. The most important information one learns from these results is that both U–C and C–C bonding are strengthened on going from configuration B to A.

Finally, a word about the conducting properties of these materials. Numerous experimental measurements prove that UC_2 is a metal, whereas CaC_2 is an insulator. What do our calculations predict? Shown in Figure 4 are the total DOS of UC_2 at left and that of CaC_2 at right. The Fermi energy indicated in the figure is for 12 electrons in the former and 10 electrons in the latter. Since ϵ_F sits in the middle part of a UC_2 band, one may conclude unambiguously that this compound is metallic. On the other hand, a gap of about 2 eV separates the filled valence and the empty conduction bands in CaC_2, characteristic of an insulating type material.

$DyCoC_2(CeNiC_2)$ Structure

The structure of $CeNiC_2$ was first reported in 1979.[26] Since then, more than 30 compounds have been found to crystallize in this form. These carbides have metallic luster and thus are expected to be metallic. Some of them are very stable in air and are possibly magnetic.[24] The space group of the $CeNiC_2$ type structure is *Amm*2, base-centered orthorhombic. It is formed by stacking alternately two-dimensional NiC_2 and distorted hexagonal rare-earth-metal sheets. Two views of a sample $DyCoC_2$ compound are depicted in Figure 5. The two short Co–C distances are 1.95 and 1.98 Å, and there is no Co–Co bond in the structure. Carbon atoms form dimeric units with a carbon–carbon separation of 1.37 Å, a little longer than a typical C–C double bond.

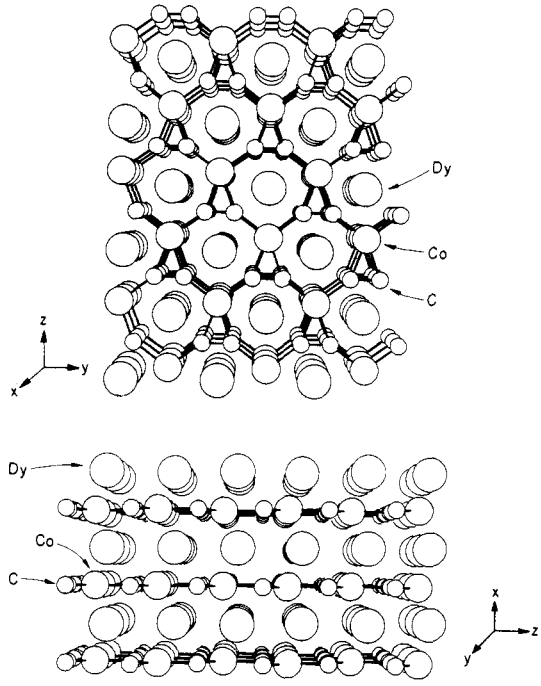

Figure 5. Two persepective views of the $DyCoC_2$ structure. The top view is seen along the *a* axis and the bottom view along the *b* axis.

The $CeNiC_2$ structure is closely related to the YCoC type,[48] whose electronic structure we have studied.[72] This compound can also be considered as a layered one with alternating CoC and Y sublayers. The CoC sheet is actually composed of parallel ···Co–C–Co–C–Co··· chains, and the separations between these chains are large. The chain axes of the neighboring CoC layers are perpendicular to each other. The upper part of **5** shows a unit cell of YCoC.

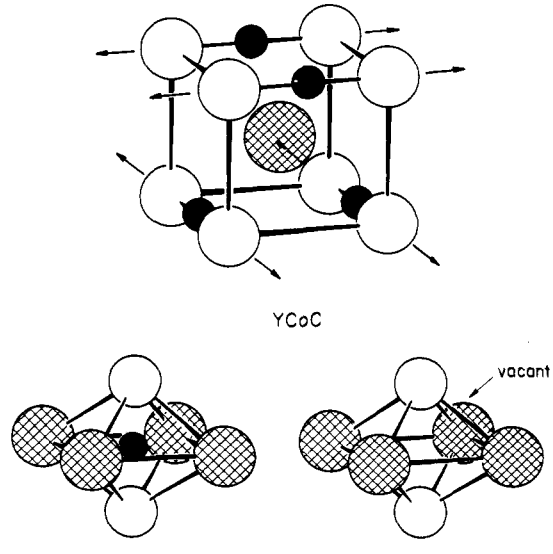

5

Arrows indicate the extended chain directions. One sees that each carbon atom is located in an octahedral hole

(72) Li, J.; Hoffmann, R. *J. Am. Chem. Soc.* **1987**, *109*, 6600.

formed by four yttrium atoms in equatorial positions and two cobalts in axial sites. Only one-half of these holes are occupied by carbon atoms; the other half are vacant. These are drawn in the lower portion of **5**. Naturally, one thinks about the possibility of filling up the other half of the holes with carbon and generating a new type of carbide, $YCoC_2$. Such a process is demonstrated graphically in **6**. For the

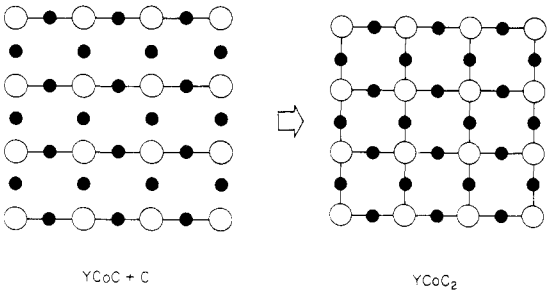

6

sake of clarity, only one sublayer is shown. What one obtains is then a square lattice. Each cobalt is coordinated to four carbons, and each carbon is two-coordinated by cobalt atoms. In fact, such a coordination environment has been observed in a number of crystal compounds, including ideal perovskite structure of ABO_3 and ABX_3,[10] K_2NiF_4 structure,[73] and copper oxide superconducting materials, such as newly synthesized $Tl_2Ca_2Ba_2Cu_3O_{10}$,[74] as well as in cluster type M_4F_{20} moieties (M = W, Mo, Ta, and Nb).[75]

Instead of forming the "ideal" $YCoC_2$ structure described above, the real geometry of $YCoC_2$ (a $CeNiC_2$ type) is a distorted form of the idealized one, as shown in **7**. Such

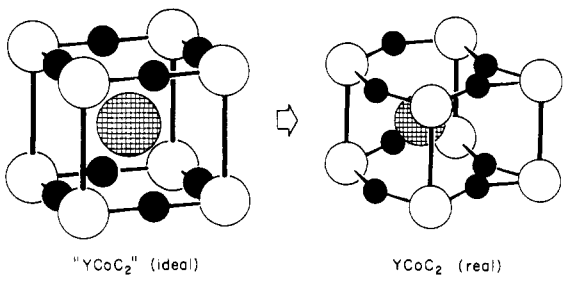

7

distortion leads to "pairing" of carbon atoms, **8**, and the coordination environment of cobalt atoms so obtained is analogous to that of Pt in molecular $L_2Pt(C_2R_2)$ entities such as $(Ph_3P)_2Pt(C_2Ph_2)$[76] and $(Ph_3P)_2Pt(C_6H_8)$.[77]

A close look at the $CeNiC_2$ structure reveals (1) that the system is selective in electron count, only 19–21 electron species are found so far, and (2) that the transition metals are limited to group VIII Fe, Co, and Ni atoms. Early transition-metal carbides of the same composition do not exist in this crystal form.[35] We would like to understand what the electronic driving force is for the "pairing" and what gives rise to selectivity in both the type of participating element and the number of electrons in the structure.

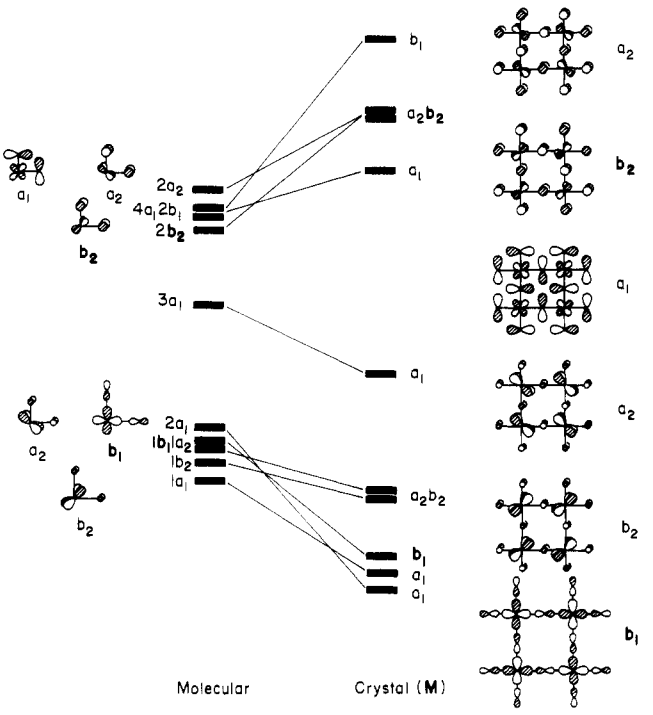

Figure 6. Correlation diagram of orbitals of a ML_2 molecule ($\angle L\text{–}M\text{–}L = 90°$) and those of a ML_2 2D square lattice at $\mathbf{k}$ = (0.5, 0.5, 0.0). Orbitals are sketched in the figure, and their symmetries are labeled beside the energy levels.

Our approach is to exclude the rare-earth metals in the first part of the analysis. Although R–T and R–C interactions in these systems should not be neglected, they are certainly not the driving force for the distortion because it seems that no matter what effect these metals may have on the systems, it is similar in both ideal and real structures, since the R–T and R–C distances are approximately the same in the two. In fact, R–C is 2.65 Å in both structures for R = Dy. We will see that it is the CoC_2 sublattice that is important in affecting the structural stability of this class. A full structure including the rare-earth elements will be considered in a later section.

Let us begin with the hypothetical ideal structure, the two-dimensional CoC_2^{3-} square lattice. This is drawn at left in **9**. The shaded area in **9** defines the unit cell, and

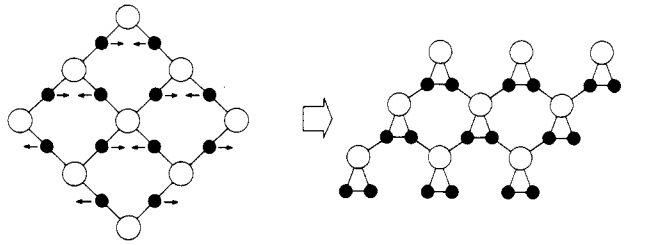

8

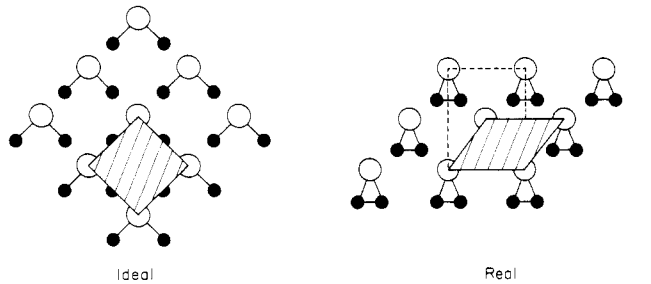

9

(73) Galasso, F.; Darby, W. *J. Phys. Chem.* **1963**, *67*, 1451.
(74) Hazen, R. M.; Finger, L. W.; Angel, R. J.; Prewitt, C. T.; Ross, N. L.; Hadidiacos, C. G.; Heaney, P. J.; Veblen, D. R.; Sheng, Z. Z.; Ali, A. El; Hermann, A. M., submitted for publication.
(75) (a) Edwards, A. J.; Peacock, R. D.; Small, R. W. *J. Chem. Soc.* **1962**, 4486. (b) Edwards, A. J. *Ibid.* **1964**, 3714.
(76) Glanville, J. O.; Steward, J. M.; Grim, S. O. *J. Organomet. Chem.* **1967**, *7*, 9.
(77) Bennett, M. A.; Robertson, G. B.; Whimp, P. O.; Yoshida, T. *J. Am. Chem. Soc.* **1971**, *93*, 3797.

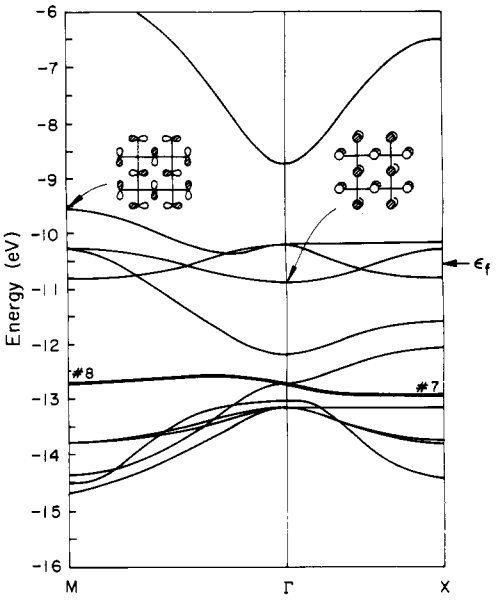

Figure 7. Band structure of a square planar CoC_2 lattice along MΓ and ΓX lines in the first Brillouin zone. Two carbon lone-pair orbitals are drawn in the figure. Band no. 8 along MΓ and no. 7 along ΓX are labeled. The Fermi energy calculated for 20 electrons is indicated by an arrow.

that each cell contains one CoC_2 unit is emphasized in the drawing. The C–Co–C angle within each unit is 90°. At right in **9** is the distorted or real structure. It is a centered rectangular lattice in 2D. The primitive cell of this lattice contains also one CoC_2 unit and its area (volume if 3D) is shaded. We shall come back to this structure in the next section.

The C_{2v} ML_2 molecular orbitals can be easily derived,[78] and they are sketched in **10** for M = Co, L = C, and the

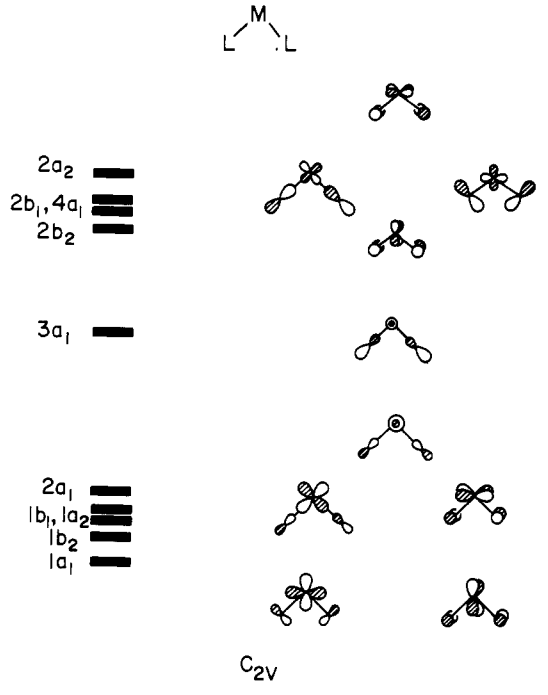

10

L–M–L angle θ = 90°. The lower energy block is a set of M–L bonding orbitals and the higher energy one, M–L antibonding orbitals. One may notice immediately from **10** that the metal–carbon bonding orbitals are more concentrated on the metal atoms, whereas the antibonding ones are weighted more on carbon atoms. This is the reverse of what one usually encounters in transition-metal complexes but is not a surprise. One observes such reverse when dealing with transition metals of low d-orbital energy or ligands of high p-orbital energy. To generate the corresponding crystal orbitals, we turn on nearest-neighbor interactions. This leads to what is presented in Figure 6 at the M point in the Brillouin zone. Some orbitals are lowered, others are raised, but the general features are retained. For example, nearest-neighbor interactions between $1b_1$ states at this point give a positive overlap between the parent cell and its bordering one and thus stabilize this orbital. $2b_2$, on the other hand, is raised because of its antibonding character between the neighboring cells. Energy bands along symmetry lines M–Γ and Γ–X of the first Brillouin zone are plotted in Figure 7. Bands of the lower block (~–12.7 eV → –14.7 eV) are M–C bonding, except one band: no. 8 along MΓ, no. 7 along ΓX, which starts with metal d_{z^2} and carbon p antibonding at M and gradually becomes d_{z^2} nonbonding at X. Crystal orbitals of this band at the two k points are sketched in **11**. Bands

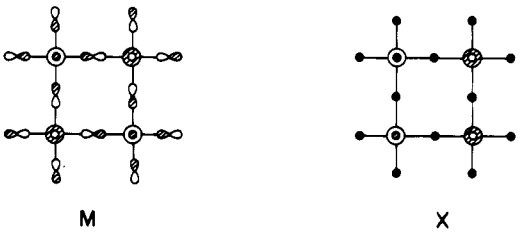

11

between –9.5 and –12.2 eV are either C–C nonbonding or M–C antibonding. For a square-planar ML_4 molecule of D_{4h} symmetry, there will be a set of nonbonding ligand (L) lone-pair orbitals, **12**.[79] Symmetry does not allow mixing

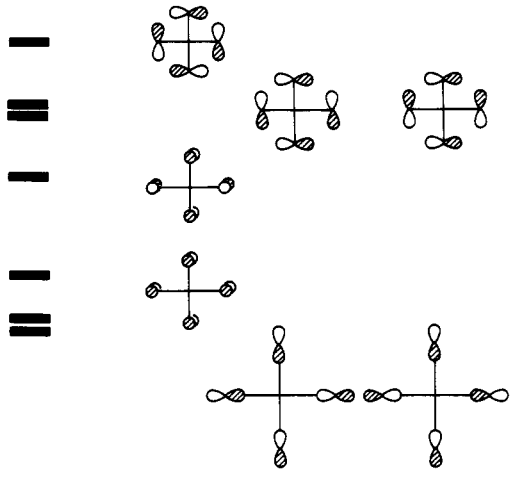

12

of the metal d's into these lone-pair orbitals. Analogous orbitals must exist in a two-dimensional square lattice with ML_4 as the building block. Indeed this is seen in the energy bands as well as in the projected density of states.

(78) Albright, T. A.; Burdett, J. K.; Whangbo, M.-H. *Orbital Interactions in Chemistry*; Wiley: New York, 1985.

(79) (a) Underwood, D. J.; Nowak, M.; Hoffmann, R. *J. Am. Chem. Soc.* **1984**, *106*, 2837. (b) Wheeler, R. A.; Whangbo, M.-H.; Hughbanks, T.; Hoffmann, R. *Ibid.* **1986**, *108*, 2222.

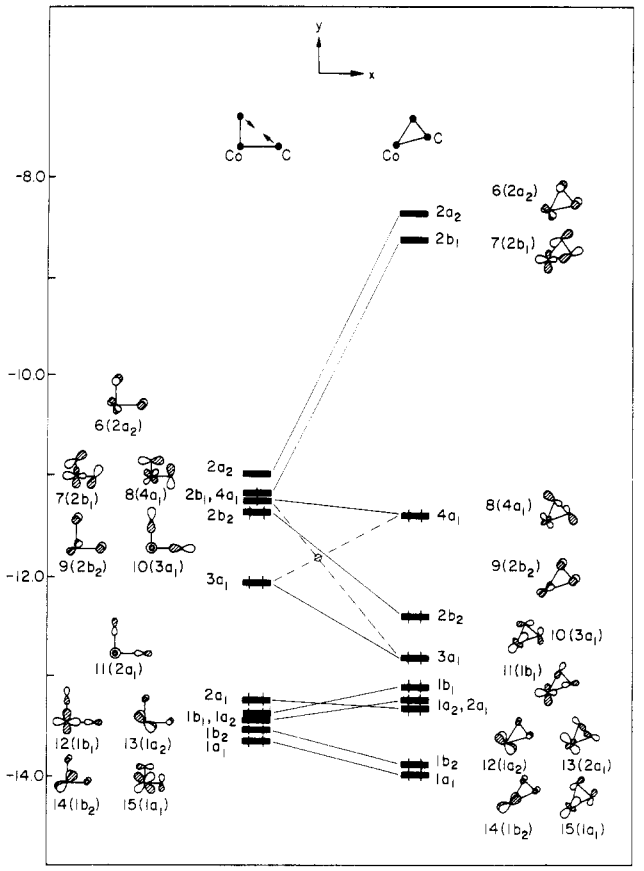

Figure 8. Schematic diagram correlating two ML_2 molecules. On the left are orbitals of ML_2 with $\theta = 90.0°$ and on the right, those with $\theta = 40.7°$. The actual orbital correlations are made with solid lines, the dashed lines show avoided crossings.

Two such lone-pair crystal orbitals are drawn in Figure 7. Later on, when we compare the ideal and distorted lattices, we shall see the importance of these orbitals to the structural stability. The Fermi energy for 20-electron CoC_2^{3-} is computed to be −10.55 eV, falling right among these bands.

Orbitals of the distorted CoC_2^{3-} lattice can be obtained conveniently from those of the ideal structure. Again, we start with the molecular orbitals of ML_2 and then extend them to the solid state. For a CoC_2 unit with C–C = 1.37 Å the C–Co–C angle is $\theta = 40.7°$. This is much smaller than $\theta = 90°$. Figure 8 traces orbital and energy changes from $\theta = 90°$ on the left to $\theta = 40.7°$ on the right. Most remarkable is the spliting of orbitals no. $7(2b_1)$ and no. $8(4a_1)$, shown nearly degenerate for $\theta = 90°$, as the angle is decreased to the right. $4a_1$ gains a great amount of C–C bonding as the angle decreases, or equivalently, as the two carbons approach each other. At the same time, $2b_1$ becomes strongly C–C antibonding. An avoided crossing occurs between $3a_1$ and $4a_1$. The $2b_2$ orbital is also stabilized going on from $\theta = 90°$ to $\theta = 40.7°$, for similar reasons. For a 20-electron system such as CoC_2^{3-}, $2b_1$ and $4a_1$ will be half-filled at $\theta = 90°$, and the situation is a familiar first-order Jahn–Teller distortion. The $\theta = 40.7°$ geometry is favored over $\theta = 90°$. The magnitude of the energy changes is quite different for orbitals of lower energy than those of higher energy. This can be seen clearly from Figure 8. In the M–C bonding region, the energy variations are small, in contrast with the dramatic level shifts in the M–C antibonding region. This can be simply understood from **13**. The M–C bonding orbitals are concentrated on the metal atom so they are little affected by the angle change. In contrast, the metal–carbon antibonding orbitals have large contributions on carbon atoms, so they are greatly affected as θ gets smaller. It would be equally simple to generate the CoC_2 orbitals by an FMO (fragment molecular orbital) analysis, in which one considers a metal atom interacting with a bonded C_2 fragment. Some of the C_2 fragment orbitals are shown in **3**. The same results as those shown in Figure 8 will be obtained.

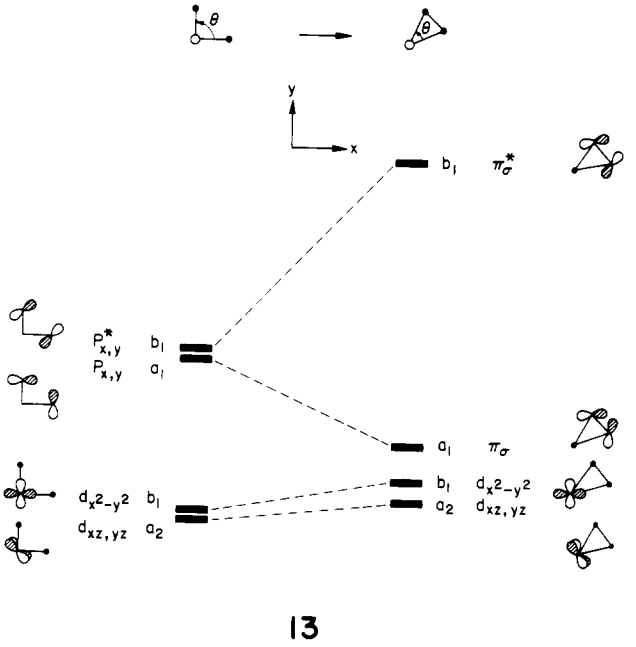

13

We now go on from the discrete molecule to the extended structure. First we plot out the energy bands along symmetry lines M → Γ → M′ in Figure 9. The Brillouin zone of the centered rectangular lattice is a distorted hexagon as shown in **14**. Crystal orbitals at M and Γ of the Brillouin zone are drawn in the figure (only the CoC_2 unit is shown). They certainly bear a resemblance to the corresponding molecular orbitals. There are some level shifts. For instance, MO no. $11(b_1)$ lying below MO no. $9(b_2)$ (see levels drawn at left of **15**) becomes crystal orbital no. 9 at Γ and is above no. 7 at the same k point, which is derived from MO no. 9. Clearly, these shifts are due to near neighbor interactions. MO no. $12(a_2)$ is mainly $3d_{xz}$ of Co. This orbital stays nearly unaffected during the process because of small contributions from carbon atoms.

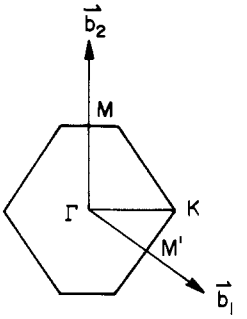

14

Comparing Figure 7 with Figure 9, one immediately realizes the features that distinguish the two. The Fermi energy is at the top of the valence band in Figure 9, and there is a big gap between the filled and unfilled levels. In Figure 7, however, ϵ_F falls right in the middle of the band so there is no bandgap.

In the square-planar lattice, most of the carbon lone-pair orbitals are distributed in the region around the Fermi level and are partially filled. Upon distortion (or pairing),

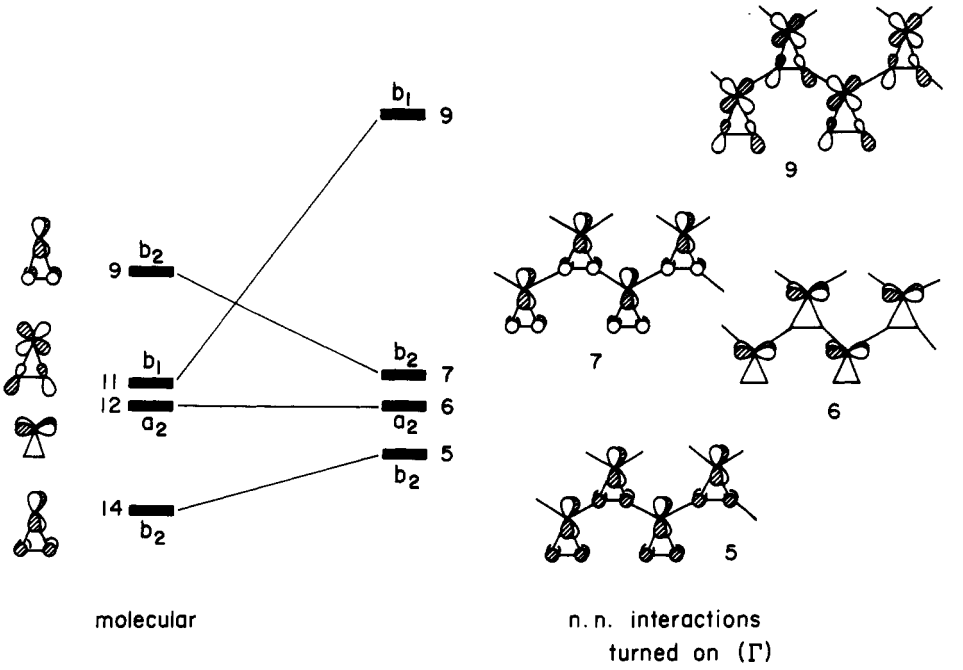

15

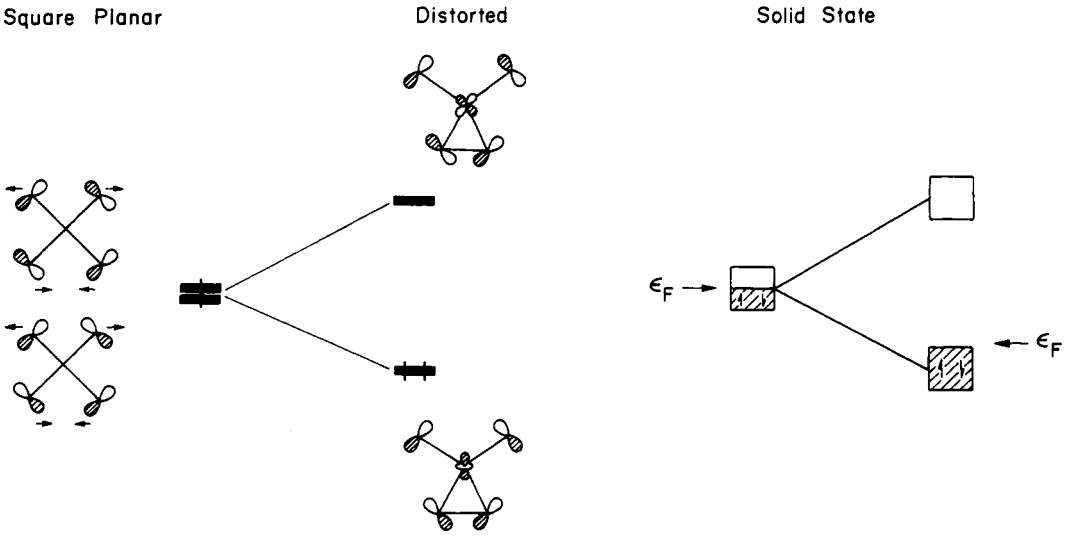

16

they split into carbon–carbon bonding and antibonding sets. A gap is then created between the two sets. With a 20-electron count, the bonding orbitals are completely filled, and the system gains its maximum stabilization. The molecular Jahn–Teller distortion finds its analogue in a Peierls-type deformation of the extended material.

16 compares the molecular and extended systems. When more electrons are added, we expect a switch of the geometrical preference since one starts to fill up the C–C antibonding orbitals in Figure 9, which are higher in energy than those nonbonding orbitals in Figure 7. Plotted in Figure 10 is the average total energy difference of the two structures vs electron count. For the systems that have been reported with 19 → 21 electrons, the structure with dimeric C_2 units is favored by the extended Hückel calculations. For electron counts higher than 21, the square-planar lattice should become more favorable. Ternary metal carbides of the RTC_2 type with such high electron counts have not yet been made. It would be interesting to see them; of course, they might adopt geometrical structures other than those examined here.

A number of density of state curves for the two structures are depicted in Figures 11 and 12. The projections in Figure 11 are the DOS of the square-planar lattice. The Co 3d orbitals are shown in the right panels, and the carbon states in the left side. Each Co 3 d orbital splits nicely into two peaks: the Co–C bonding states at lower energy and the Co–C antibonding states at higher energy. The splitting of $3d_{x^2-y^2}$ in Figure 11c is larger than that of $3d_{xz}$ and $3d_{yz}$ in Figure 11a and $3d_{xy}$ in Figure 11b, since the metal–carbon interaction of the former is σ-type, whereas π-type interactions are responsible for the latter. These interactions are shown schematically in Figure 13 in the same way as in Figure 11. As expected, each 3d orbital of cobalt contributes a larger percentage in the bonding region. Note also how the carbon lone-pair orbitals show up in the density of state curves in the left panels. They are designated as $n_C(a)$, $n_C(b)$, and $n_C(c)$ in Figure 11. Let us take a little closer look at these nonbonding orbitals.

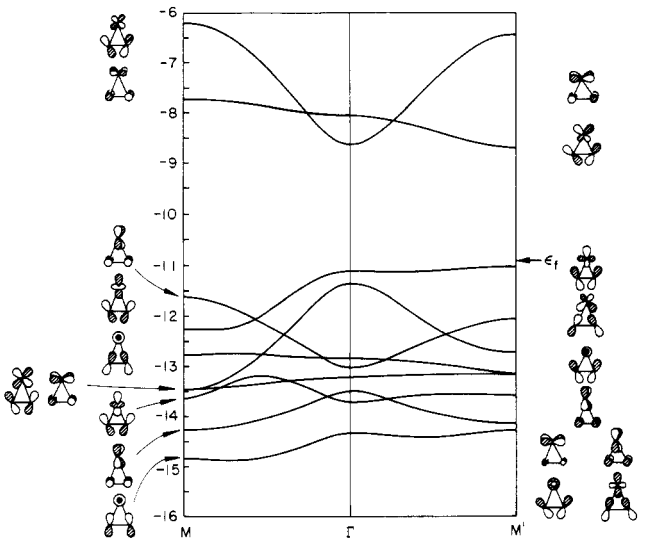

Figure 9. Band structure of the two-dimensional CoC_2^{3-} lattice. Bands are plotted along MΓ and ΓM′ in the first Brillouin zone. Crystal orbitals at M and Γ are sketched in the figure. The Fermi energy is shown by an arrow.

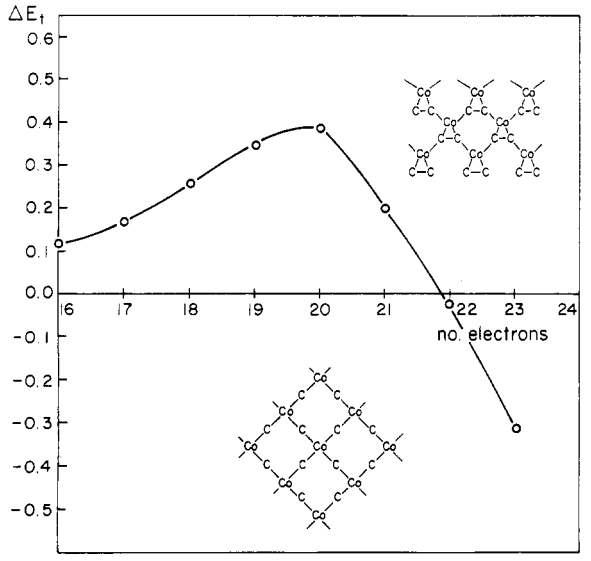

Figure 10. Average total energy change ΔE_t for the two CoC_2 2D structures. The curve is plotted as the difference between E_t of the square lattice and that of the centered-rectangular lattice for several electron counts.

What is projected out at left of Figure 11b is actually the sum of a p_y orbital of the first carbon and p_x of the second C. Crystal orbitals of various phase combinations, such as those given in **17**, all contribute to this projection.

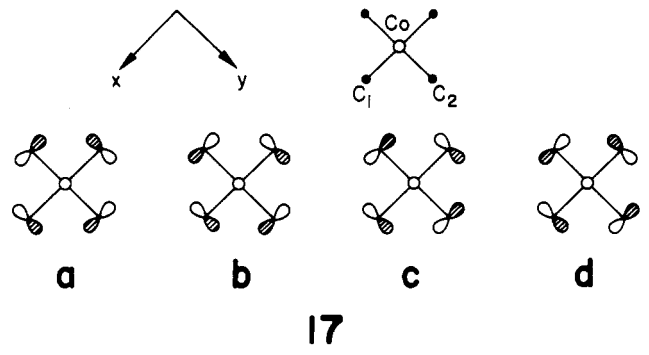

17

17a has the proper symmetry to interact with Co $3d_{xy}$,

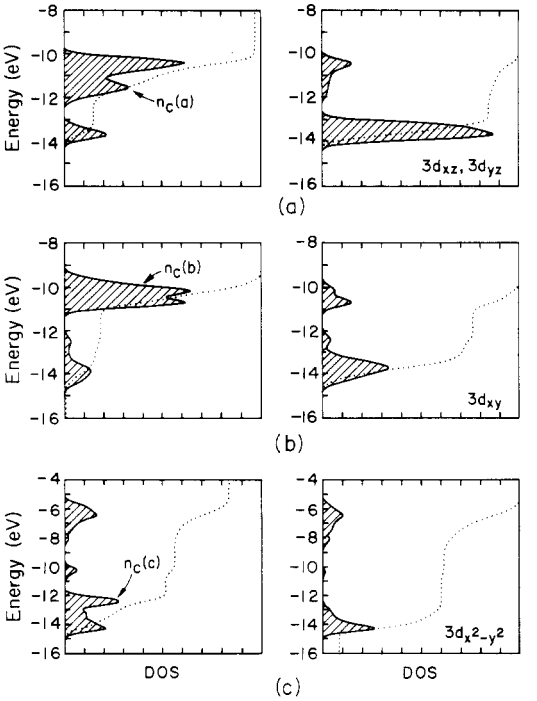

Figure 11. DOS curves (shaded area) for the CoC_2 square lattice: (a) orbitals that contribute to the bonding of carbon 2p combinations with metal $3d_{xz}$ and $3d_{yz}$, (b) with metal $3d_{xy}$, and (c) with metal $3d_{x^2-y^2}$. Projections of carbon orbitals are shown in the left panels and those of the metal orbitals at right. Carbon lone-pair orbitals are labeled as $n_C(a)$, $n_C(b)$, and $n_C(c)$. Dotted lines are integrations of the projected DOS.

resulting in Co–C bonding and antibonding levels. **17b–d**, on the other hand, do not interact with any Co 3d orbitals, due to symmetry reasons, and become nonbonding. They are the main contributors to the upper part of the band centered between −9.0 and −11.0 eV. Figure 14 helps to make the point clearer. In this figure, only the *positive* combination of $p_y(C_1)$ and $p_x(C_2)$ is plotted out, so that contributions from **17c** and **17d** are eliminated. Superimposing this figure onto the left panel of Figure 11b, we see that the peak at ∼−10.2 eV (labeled $n_C(b)$) in Figure 11b is missing in here. This has to be attributed to the nonbonding orbitals of **17c** and **17d** type. $n_C(a)$ in Figure 11a and $n_C(c)$ in Figure 11c may be understood in a similar way. For the real structure, separate DOS projections of Co $3d_{yz}$ with the C_2 π_z orbital and $3d_{xz}$ and $3d_{xy}$ of Co with π^* of C_2 are plotted in Figure 12, parts a and b, respectively. They are labeled in the lower right corner of each panel. As in the square-planar case, 3d orbitals of cobalt split into bonding and antibonding peaks. The C_2 π_z orbital drawn in Figure 12a is nearly completely filled for a 20-electron count. This is analogous to what happened in Figure 8 for a molecular CoC_2 (cf. orbital no. 9 in Figure 8). The π^* states of the C_2 dimer, sketched in **18**, are

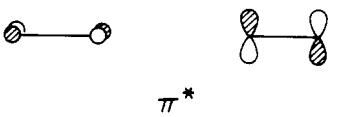

π^*

18

projected in the middle panel of Figure 12b. These states are characterized by three peaks: two at higher energy (−6.5 and −8.5 eV), and one spread out between −11.0 and −15.0 eV. These are contributions to the π^*–$3d_\pi$ bonding (lower energy peak) and π^*–$3d_\pi$ antibonding (higher energy peaks). No ambiguity arises in assigning the π^*–$3d_\pi$ an-

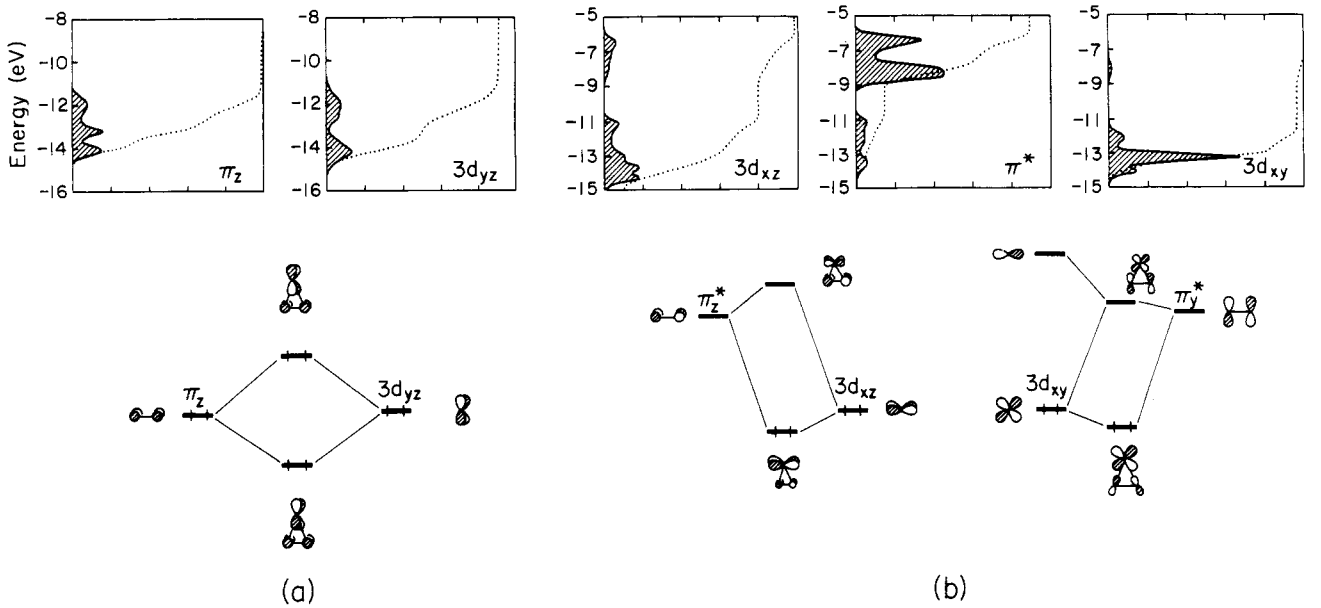

Figure 12. Projected DOS in the 2D CoC_2 structure: (a) π_z of carbon and $3d_{yz}$ of cobalt; (b) π^* of carbon and cobalt $3d_{xz}$ and $3d_{xy}$. Shaded areas are the orbital contributions to the total DOS and dotted lines, integrations. A schematic interaction diagram is drawn at lower portion of each panel.

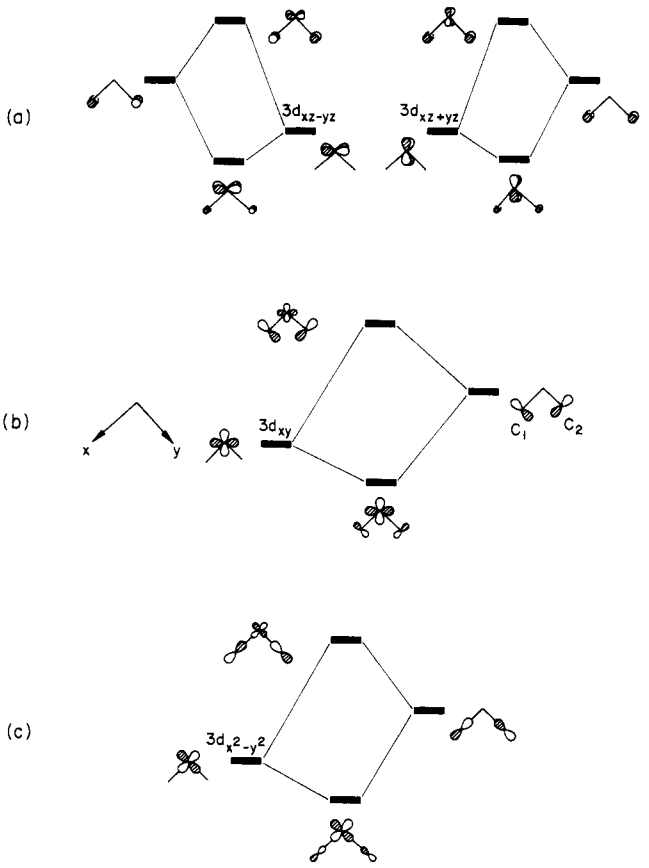

Figure 13. Schematic diagrams showing some metal–carbon orbital interactions in CoC_2 2D square lattice. From top to bottom, they are carbon 2p states with (a) metal $3d_{xz}$ and $3d_{yz}$, (b) metal $3d_{xy}$, and (c) metal $3d_{x^2-y^2}$.

tibonding orbitals to the two upper peaks; the peak at −6.5 eV is apparently the π_z^*–$3d_{xz}$ antibonding, and the peak at −8.5 eV is π_y^*–$3d_{xy}$ antibonding. The fact that π_y^*–$3d_{xy}$ antibonding levels lie lower in energy is due to mixing of the metal p_x orbital, which enters in a bonding way toward π_y^*, thus stabilizing the π_y^*–$3d_{xy}$ antibonding orbitals. The schematic orbital interaction diagrams inserted in Figure 12 help in understanding the picture described above.

COOP (crystal orbital overlap populations) curves[80] of Co–C and C–C bonding for the real structure can be found in Figure 15. The ϵ_F marked in the figure corresponds to a 20-electron system. Maximum bonding for both Co–C (op = 0.4, op = overlap population) and C–C (op = 1.5) is achieved with this electron count, in accordance with the average total energy change shown in Figure 10. Two distinct peaks are seen for each of the two π states in the bonding region of the C–C curve as well as for π^* states in the antibonding area of the same curve. They correspond to π–3d bonding and antibonding, π_y^*–d_{xy} antibonding and π_z^*–d_{xz} antibonding. The contribution of π^* to the π^*–$3d_\pi$ bonding states should show up between −11.0 and −15.0 eV but it is so small that it is "eaten" by the π state in the same energy region.

The analysis that we have made so far has been limited to two-dimensional structures without including Dy atoms in the calculations. The reasons for this simplification have been given at the beginning of the section. To support this approximation, we compared the average total energy difference between the two structures, ideal and real, in two-dimensional CoC^{3-} lattice and in three-dimensional $DyCoC_2$. The results are remarkably similar.

One might think of other possible distorted forms for the RTC_2 structure. Two are given in **19**. **19a** is generated by making alternating short and long Co–C bonds in the

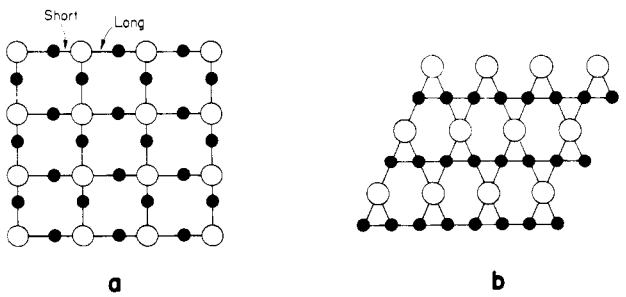

19

(80) Hoffmann, R. *Angew. Chem., Int. Ed. Engl.* **1988**, *26*, 846.

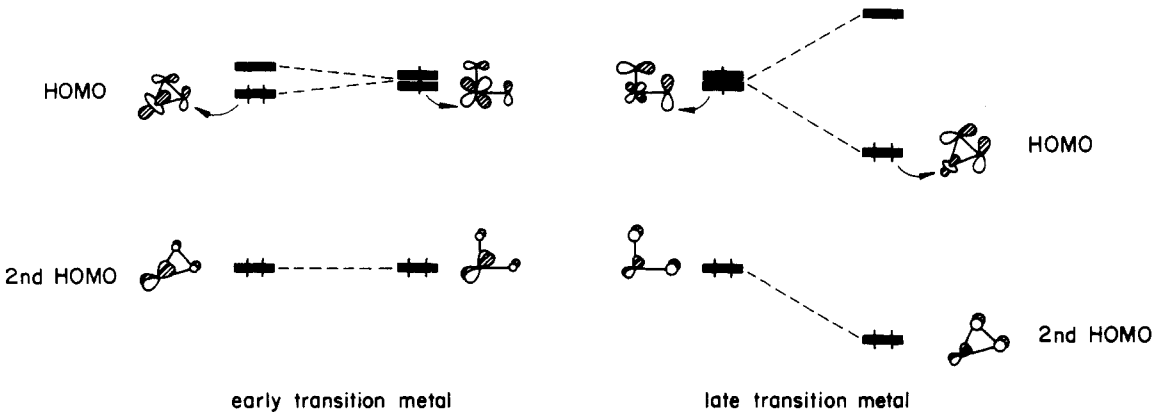

20

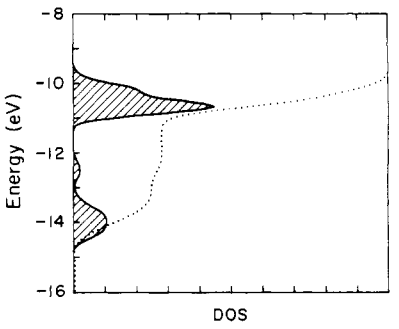

Figure 14. DOS projection of positive combination of $2p_y$ orbital from the first carbon and $2p_x$ from the second carbon in the unit cell. Dotted line gives integration of this state.

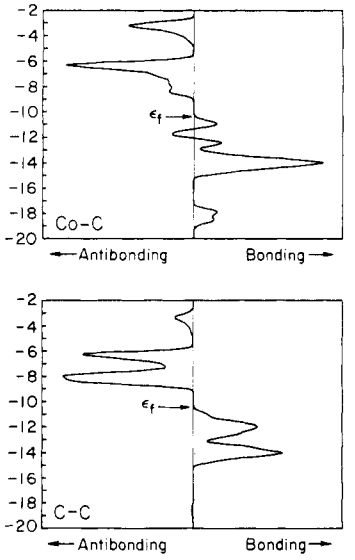

Figure 15. Crystal orbital overlap populations (COOP) of Co–C bond and C–C bond. ϵ_F is calculated for 20 electrons and is indicated in the figure.

CoC_2 layer, and **19b** is obtained by forming a kagomé net of equal C–C bond length. The geometrical arrangement in **19a** has been found in many distorted perovskite structures[81] as well as other compounds such as $(MoNCl_3)_4$[82] and α-$VOPO_4$.[83] In Figure 16, the relative stability

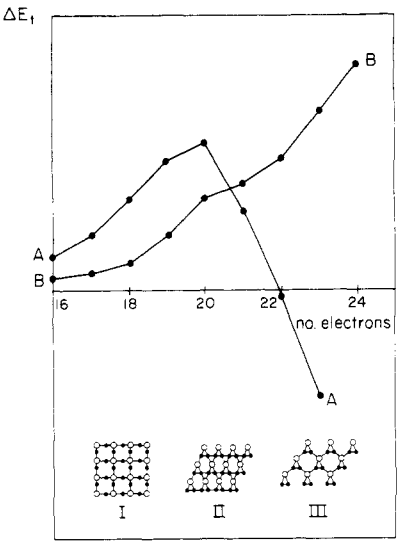

Figure 16. Variations of the total energy change versus number of valence electrons. Curve A plots $\Delta E_t = E_t(I) - E_t(III)$ and curve B, $\Delta E_t = E_t(II) - E_t(III)$. Structures of I, II, and III are shown at the bottom of the plots.

of such different lattice forms is compared as a function of electron count. The energy difference between **19a**, I, and the real form, III, is plotted in curve A. Curve B plots the same for **19b**, i.e., $E_t(II) - E_t(III)$. For electron counts of 16–21, III is always favored. For higher electron counts, however, there is a switch in curve A, that is, I becomes more stable than III.

It should be noted that the details of our figures showing geometrical preferences as a function of electron count may be sensitive to the parameters and extended Hückel methodology. Nevertheless we think the general features of the trends emerge even from these approximate calculations.

Ternary metal carbides RTC_2 with early transition-metal elements of lower electron count do not exist in $DyCoC_2$ crystal form. Those known to date belong to the $UMoC_2$ type.[35,38] This structure also has metal and carbon atoms in the same layers. The metal–carbon bonds are short, for example, 2.16 Å (average) in $UMoC_2$.[38] No short carbon–carbon contact is found. Compounds of this class differ from $DyCoC_2$ in that the transition-metal elements in the

(81) (a) Müller, O.; Roy, R. *The Major Ternary Structural Families*; Springer-Verlag: Berlin, 1974; pp 174ff. (b) Galasso, F. S. *Structure Properties, and Preparation of Perovskite-Type Compounds*; Pergamon Press: Oxford, 1969. (c) Straumanis, M. E. *J. Am. Chem. Soc.* **1949**, *71*, 679.

(82) (a) Strähle, J. *Z. Anorg. Allg. Chem.* **1970**, *238*, 375; **1971**, *90*, 380. (b) Dehnicke, K.; Strähle, J. *Angew. Chem.* **1981**, *93*, 451; *Angew. Chem., Int. Ed. Engl.* **1981**, *20*, 413. (c) Griffith, W. P. *Coord. Chem. Rev.* **1972**, *8*, 369.

(83) Jordan, B.; Calvo, C. *Can. J. Chem.* **1973**, *51*, 2621.

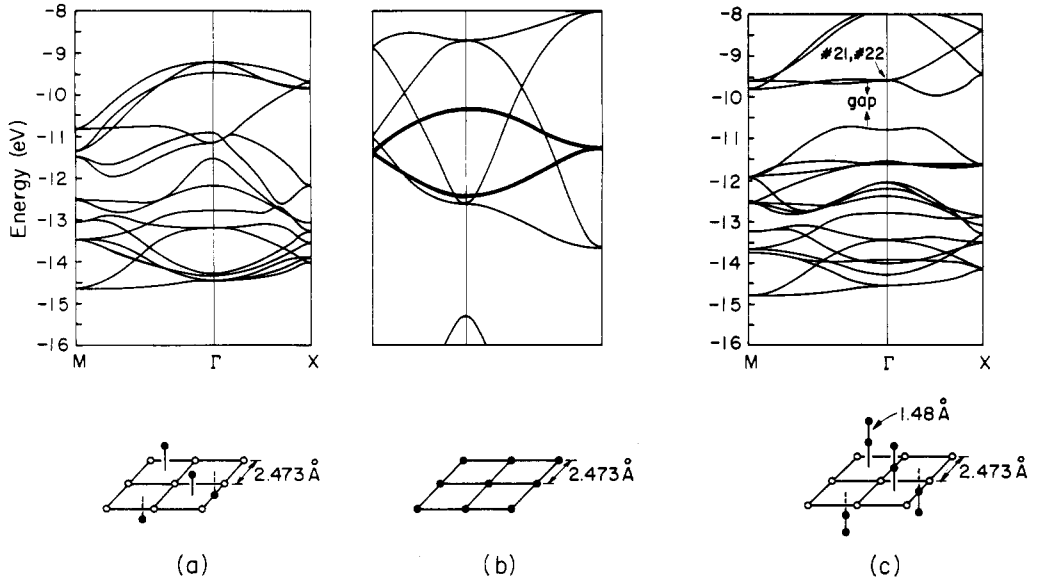

Figure 17. Band structure for (a) CoC 2D lattice, (b) carbon square lattice, and (c) CoC_2 2D layered structure. Carbon p_z bands are drawn with heavy lines in (b). The lattices are shown below the band structure plot. Selected interatomic distances are given.

structure are more electropositive. They have higher atomic d-orbital energies relative to the carbon 2p orbitals and are more easily oxidized. The smaller number of valence d electrons gives rise to lower electron counts (17–19), compared to the $DyCoC_2$ structure. What consequences does this difference lead to? **20** gives an answer. In the central part of **20**, orbitals that are important in this context are drawn for a MC_2 unit with M being an early transition metal at left and a late transition metal at right. With late transition metals such as Fe, Co, and Ni, these orbitals come mainly from the 2p of the C_2 unit. The opposite situation occurs for early transition metals like Cr, Mo, and W: it is the d orbitals that make a larger contribution to these orbitals. Upon distortion or pairing, a C–C bond is formed for either structure. As we have discussed previously, in the case of late transition metals the two orbitals shown in the drawing are greatly stabilized because of large positive overlap between the two carbon atoms. Such stabilization is not observed for the case of the early transition metals. The two orbitals under consideration stay very much the same during the process, since they are metal centered and are very little affected by the formation of carbon pairs. Thus, the $DyCoC_2$ structure is not favored for early transition-metal carbides with a RTC_2 composition.

$UCoC_2$ Structure

Having discussed the bonding and structural stability in $DyCoC_2$, we now turn to another ternary RTC_2 metal carbide, the tetragonal $UCoC_2$ structure, whose unit cell is illustrated in **21**. The known compounds are $UCoC_2$, $UFeC_2$, $UNiC_2$, $PuCoC_2$, $ScCoC_2$, $ScFeC_2$, and $ScNiC_2$.[19,22,23,84] The square lattice of Co atoms in this structure is capped by C_2 units from both sides, with a C_2 axis perpendicular to the cobalt plane. Although sitting in crystallographically equivalent 2c sites, the coordination environments of the two carbons in the dimeric unit are quite different; that next to the Co square lattice is bonded to four cobalt atoms with a Co–C distance of 2.10 Å, but no short cobalt–carbon contact is observed for the other C further away from the square lattice. The C–C bond length in each C_2 pair, 1.48 Å, is longer than a double bond but short compared to a single bond. The Co–Co interatomic distance within the square lattice is a short 2.47 Å. Uranium atoms in this structure are located in the cavities of the face-sharing square prisms formed by four parallel C_2 units. The relationship of the $UCoC_2$ structure to binary CaC_2 and ternary $ThCr_2Si_2$[85] is developed in **22**. The

Table II. Calculated Total Energies in Two Possible $ThCr_2Si_2$ Structures

no. of electrons	E(I), eV	E(II), eV	E(II) – E(I), eV
22	-333.8	-336.7	2.9
23	-346.5	-349.4	2.9
24	-359.0	-361.9	2.9
25	-371.5	-374.2	2.7
26	-383.8	-386.3	2.5
27	-395.9	-398.0	2.1
28	-407.8	-409.3	1.5
29	-419.6	-420.2	0.6
30	-431.2	-430.9	-0.3
31	-441.7	-441.3	-0.4
32	-451.7	-451.4	-0.3

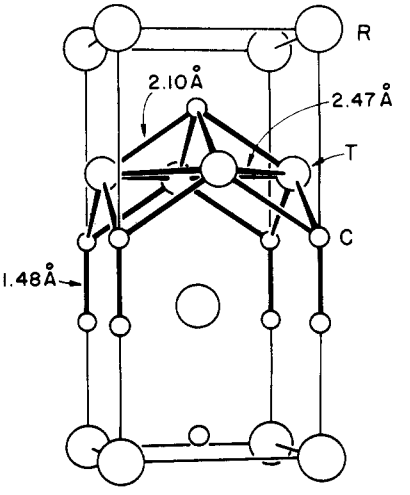

21

(84) In a recently published paper, Jones et al. disagree with the structure of $UFeC_2$ previously reported by Gerss and Jeitschko. See: Jones, D. W.; McColm, I. J.; Yerkess, J. *J. Solid State Chem.* **1988**, *74*, 304.

(85) Ban, Z.; Sikirica, M. *Acta Crystallogr.* **1965**, *18*, 594.

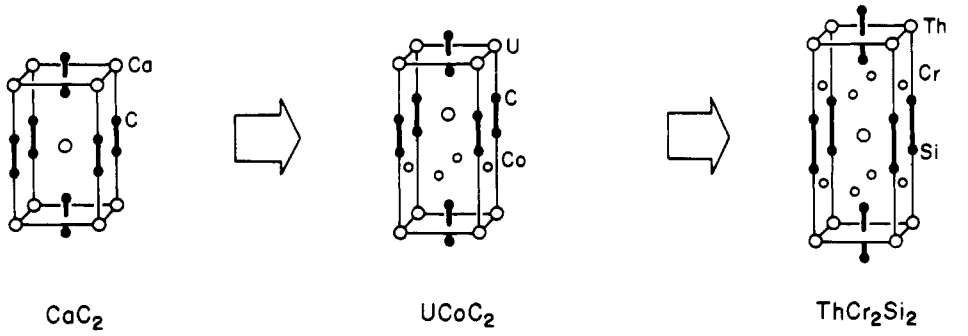

CaC_2 $UCoC_2$ $ThCr_2Si_2$

22

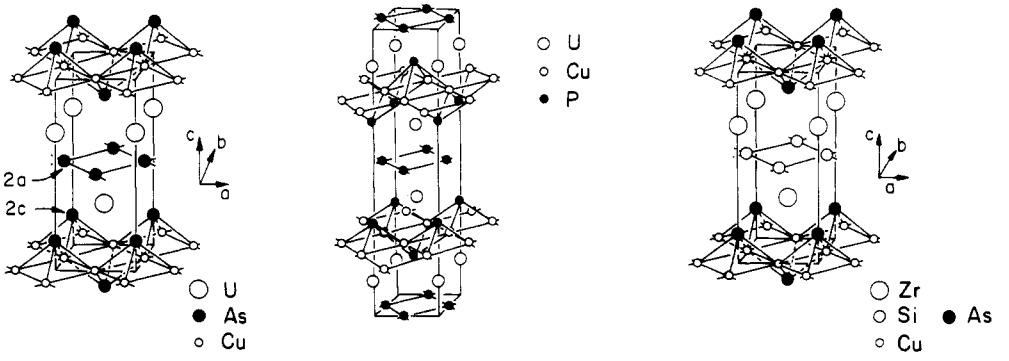

$UCuAs_2$ $UCuP_2$ ZrCuAsSi

23

$UCoC_2$ lattice can be constructed by inserting a square lattice of cobalt atoms into the void between two layers of parallel C_2 units in CaC_2. The $ThCr_2Si_2$ structure is formed by a successive insertion of another Co square lattice. $ScCoC_2$ belongs to the same crystal type as $UCoC_2$ but has a considerably shorter C–C bond of 1.26 Å. The uranium compounds are gray, with metallic luster. They are stable in air and are possibly magnetic.[19]

Closely related to $UCoC_2$ structure is a group of ternary metal pnictides. Examples of these include $UCuAs_2$,[86] $UCuP_2$,[87] and ZrCuAsSi,[88,89] whose structures are shown in **23**. $UCuP_2$ has a unit cell twice as large as $UCuAs_2$, because of slight difference in the packing pattern of the uranium atoms along the *z* direction in the two structures. In $UCuAs_2$, each U in one layer is shifted by $0.5\mathbf{a}_1 + 0.5\mathbf{a}_2$ in the next layer, whereas such a shift is made for every other U square lattice in $UCuP_2$. ZrCuAsSi, on the other hand, is a $UCuAs_2$ type structure with the As atoms in the 2a positions replaced by Si atoms. Structurally, the similarities and the differences between the $UCoC_2$ type structure and these pnictides are equally notable. First of all, a common building block, the T–M layer (T = Cu or Co, M = As or C), exists in both $UCuAs_2$ and $UCoC_2$. This layered network, shown in **24**, is formed by a square lattice of metal atoms with capping carbon or arsenic atoms sitting in the apical position of square pyramids. The metal atoms at the basal positions are tetrahedrally coordinated to four main-group elements. Second, the geometrical arrangement of uranium atoms is approximately the same in the two structures. Unlike carbon pairs in

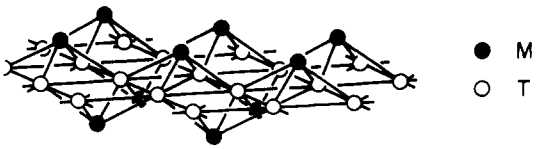

24

$UCoC_2$, As atoms take nonequivalent lattice sites, 2a and 2c. Those in 2a positions form a square lattice instead of making dimeric units with atoms in the 2c positions. The $CuAs_2$ 3D sublattice is a result of alternate packing of **24** and the As(2a) square lattice along the *z* axis. The interlayer interactions are expected to be small since the layers are so far apart from each other; the shortest As(2a)–As(2c) distance is a long 3.78 Å. Another difference is the valence electron count in the two systems. For the $UCoC_2$ type structures, the number of electrons ranges from 19 to 22. In $UCuAs_2$, it is 25, and it is 24 in ZrCuAsSi and HfCuAsSi.[88] This leads us to ask what electronic factors that might play important roles in the structural features of these compounds.

Building on the argument used in previous section, we begin with a two-dimensional approach. **25** represents a

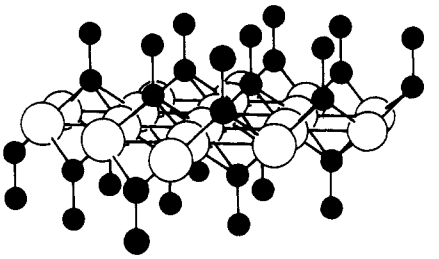

25

(86) Stepien-Damm, J.; Kaczorowski, D.; Troc, R. *J. Less-Common Met.* **1987**, 132, 15.
(87) Noël, H. *J. Less-Common Met.* **1987**, *132*, 327.
(88) Johnson, V.; Jeitschko, W. *J. Solid State Chem.* **1974**, *11*, 161.
(89) This compound does not belong to the pnictide class.

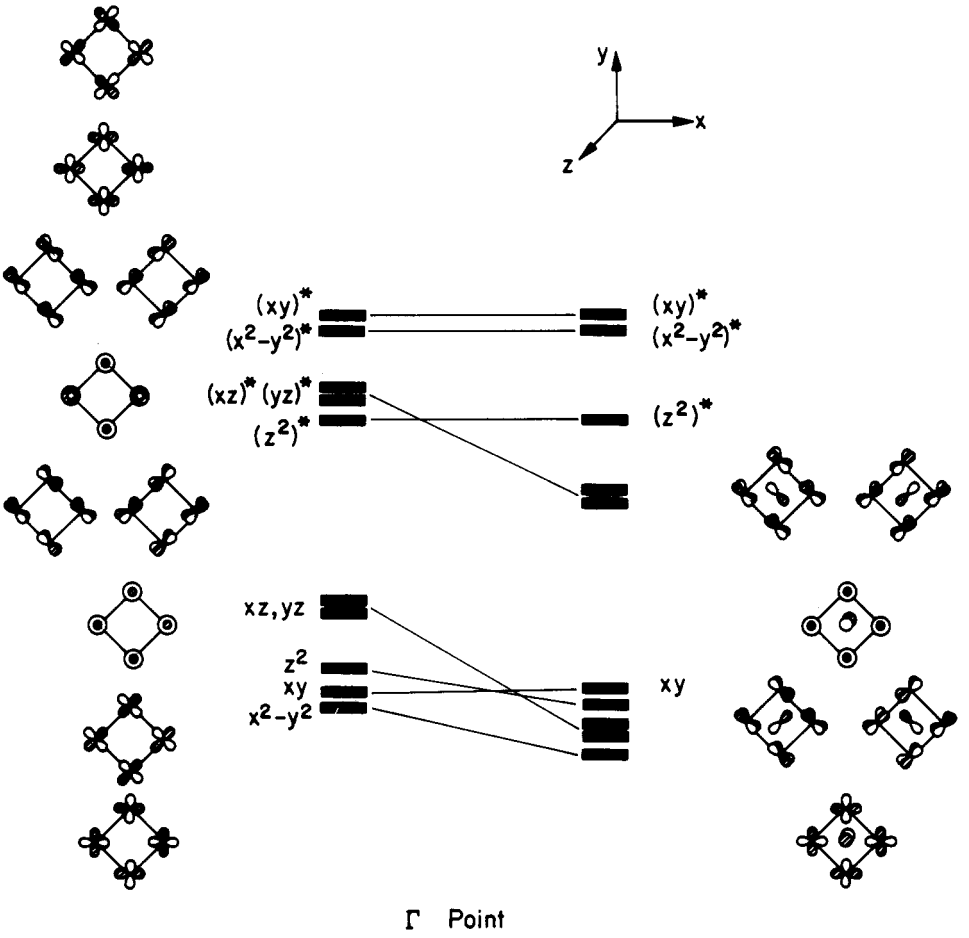

Figure 18. Metal d orbitals of a Co square lattice shown at left and the corresponding ones in CoC 2D layer (cf. **26b**) at Γ are sketched on the right. Carbon orbitals on the other side of the Co plane ($z < 0$) are not shown.

2D lattice for the $UCoC_2$ structure. Without taking U atoms into consideration, the interlayer interactions are negligible and the 2D model should be appropriate. For $UCuAs_2$, on the other hand, the two-dimensional structure is practically a layered CuAs plus an "isolated" As square lattice, as shown in **26**. Co and C parameters are actually

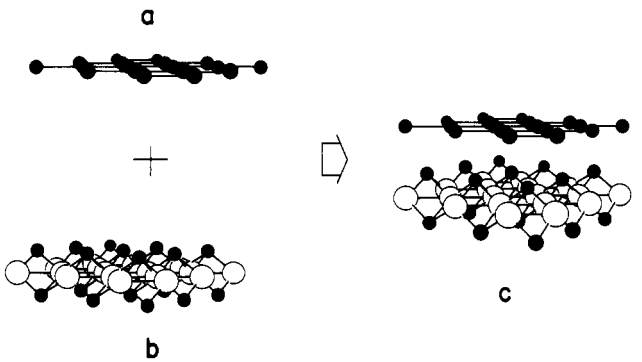

26

used in the computations. Band structures along some symmetry lines are plotted for (1) **26a**, (2) **26b**, and (3) **25**, respectively in Figure 17. The bands of **26b** are shown in the left panel. The lowest 10 are mainly metal–carbon bonding. The major contributions to these bands are from metal orbitals. Higher energy bands are attributed to metal–carbon antibonding. What about the metal–metal bonds? They certainly should not be ignored. The bonding and antibonding orbitals of metal elements penetrate the entire region of the metal–carbon states. Orbitals at one special k point, Γ, are illustrated in Figure

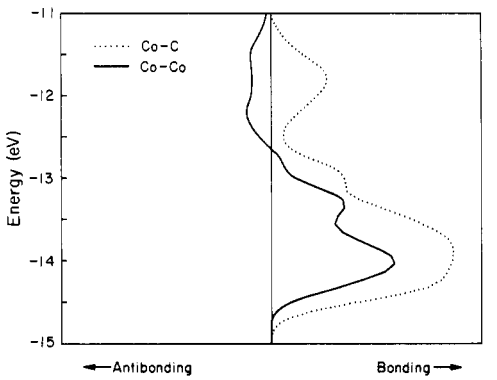

Figure 19. COOP curves of the 2D CoC lattice. The Co–Co bond is drawn with a solid line and the Co–C bond with a dotted line.

18. The metal d orbitals of a square lattice are drawn on the left side. The five bonding orbitals are well separated from the antibonding ones, leading to a five-below-five pattern. The orbitals of the square layer **26b** are those at the right-hand side of the figure, in which metal–carbon interactions are turned on. The metal $3d_{xy}$ bonding orbital, denoted by xy, and metal antibonding $3d_{x^2-y^2}$, $3d_{xy}$, and $3d_{z^2}$, labeled as $(x^2-y^2)^*$, $(xy)^*$, and $(z^2)^*$, do not have the correct symmetry to interact with carbon atoms at this point and are unaffected. Other metal d combinations are stabilized by carbon orbitals. A more complete picture is provided in the COOP curves of Figure 19. The Co–C overlap population is represented by the dotted line. It stays in the bonding region for the entire energy window shown. The solid line describes the metal–metal bond. It is in the bonding zone between ~−14.7 and ~−12.6 eV and

enters the antibonding zone for higher energies.

Returning to Figure 17, the central panel shows the band structure of a square lattice of carbon (two atoms per cell), which is a "folded-back" version of Figure 20a, the band structure of a carbon square lattice with a primitive cell description. The detailed analysis of the folding-back procedure has been given elsewhere[90] and will not be repeated here. A two-atom cell is taken here because the composite cell (**26a + 26b**) requires two cobalt atoms and two C(2c) atoms and therefore two C(2a) atoms as well. Bands that are shown in Figure 17b carry mainly the carbon 2p contributions. The p_z bands are less dispersed and are marked with heavy lines. Carbon–carbon interactions are greatly diminished, due to the large separation between the carbon atoms (2.47 Å). An approximation to the band structure of **26c** can be obtained by superimposing parts a and b of Figure 17.

Bands in Figure 17c are derived from the CoC_2 2D lattice of the $UCoC_2$ structure. As in Figure 17a, the lower energy region is mainly metal–carbon bonding. But now the two carbon atoms enter the interactions as a C_2 pair, whose orbitals are those sketched at right of **4**. They are labeled π, 3σ, and π^* here. The first is $3d_\pi$–π and 3d–3σ bonding, then the antibonding counterparts of these orbitals. The $3d_\pi$–π orbitals are depicted in **27** at the special k-point Γ.

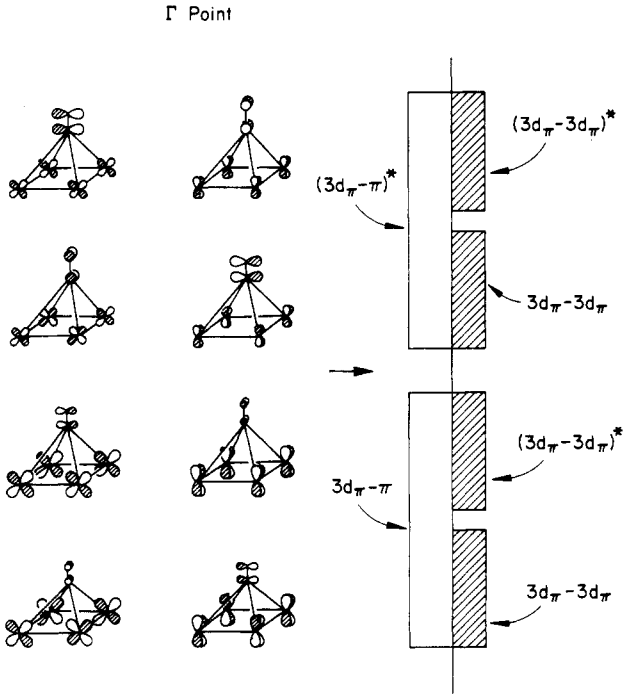

27

Here we see again how metal–metal bonding and antibonding states penetrate into both metal–carbon bonding and antibonding regions, as they do in Figure 18 and 19. The π^* orbitals act in a dual fashion. In the bands that they most contribute to, i.e., those between −8.0 and −10.0 eV, they are antibonding toward the metal d orbitals but bonding toward metal s and p levels. To see this, let us take a look at crystal orbitals no. 21 and 22 in **28**. For clarity we draw these orbitals in such a way that the metal d contributions are separated from its s and p contributions. The antibonding character between metal d and π^* is easily recognized from the two "fractional" orbitals in the upper part of **28**. The lower two pick up metal p–π^*

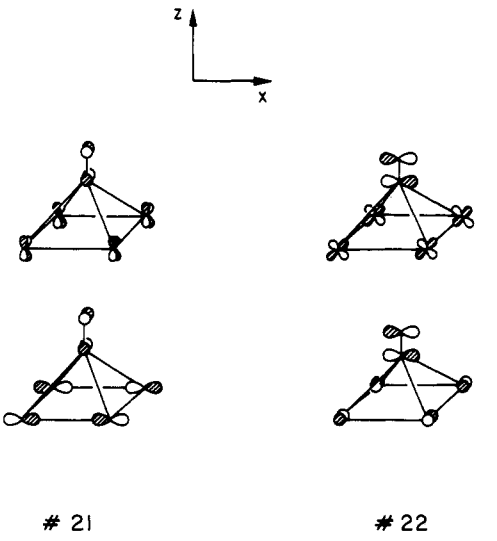

28

bonding. The extent of an AO (or FMO) contribution is reflected in the drawing by the relative sizes of the lobes.

Overall pictures of bonding in $UCoC_2$ and $UCuAs_2$ 2D structures are summarized in Figure 21, parts a and b, respectively. Obviously, for a not too high electron count, e.g., 20 electrons, where the π states are completely filled, stabilization of the system is conferred by formation of C_2 units. Both the metal d orbitals and carbon p_x, p_y orbitals that contribute to π in Figure 21a are stabilized, compared to corresponding ones in Figure 21b. The Co atoms in both structures are tetrahedrally coordination to four carbons; therefore a proper hybridization of Co s and p orbitals yields a set of symmetry-adapted orbitals that we refer to as "hollow" orbitals.[90,91] The a_1 and e combinations are shown in the figure. b_2 is omitted since it does not find a partner to interact with and will stay unchanged during the process. Being close in energy, the π^* and the e orbitals interact much stronger in Figure 21a than the carbon p_x, p_y orbitals and the e set do in Figure 21b. As a result, the π^* level is pushed down, and e goes up. The π^*–e bonding shows up nicely in the density of states projections, Figure 22. The stick in Figure 22b marks the π^* position before interaction with the e set. More than 55% of its states are lowered after the interaction is turned on. At the same time, about 80% of Co e set, shown in Figure 22c, is lifted up higher than −2.0 eV. The π^*–e bonding is the factor mainly responsible for holding together the $UCoC_2$ structure for electron counts higher than 20, since such bonding reduces the energy difference between π^* orbitals (higher) in $UCoC_2$ and the metal–carbon antibonding levels (lower) in the $UCuAs_2$ structure. Also plotted are the π orbitals of $UCoC_2$, Figure 22a. Notice the two well-separated peaks characterizing their contributions to $3d_{xz}$, $3d_{yz}$, and π bonding and antibonding states. The stick that indicates the orbital energy before metal–C_2 interactions falls almost in the middle of the two peaks. The C–C overlap population is 1.19 in $UCoC_2$, compared to 0.10 in the $UCuAs_2$ structure. The Co–C overlap population is, on the other hand, 0.30 for $UCoC_2$, a little smaller than that of 0.36 in $UCuAs_2$. This is because of filling of metal d and π antibonding states in $UCoC_2$.

Total energy difference vs electron count is plotted in Figure 23 for the two structures. The curve represents ΔE_t

(90) Li, J.; Hoffmann, R. *Z. Naturforsch.* **1986**, *41B*, 1399.

(91) Zheng, C.; Hoffmann, R. *Z. Naturforsch.* **1985**, *41B*, 292.

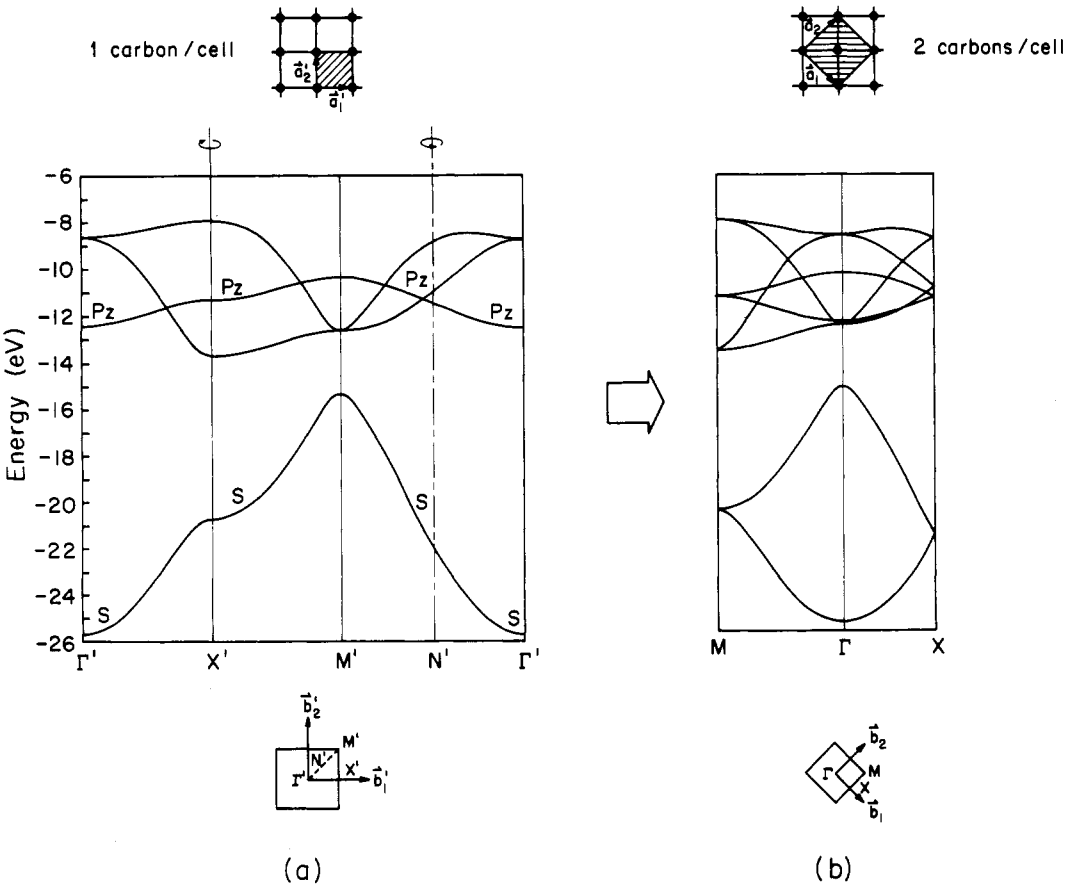

Figure 20. Band structure of a C square lattice: (a) before "folding-back" procedure and (b) after the process. The unit cell is outlined at top of each plot, and the corresponding first Brillouin zone at the bottom.

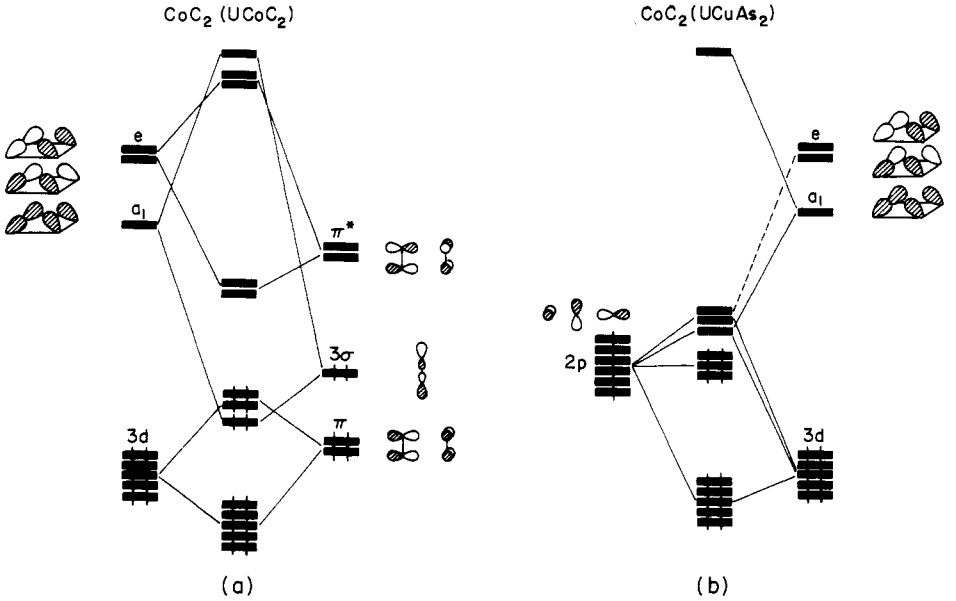

Figure 21. Schematic orbital interaction diagrams for (a) CoC_2 in $UCuAs_2$ structure and (b) CoC_2 in $UCoC_2$ structure.

$= E_t(UCuAs_2) - E_t(UCoC_2)$. $UCoC_2$ structure is favored for electron counts that give rise to positive ΔE_t values. Thus, 24 is the turning point; systems with 23 electrons or less should prefer the $UCoC_2$ structure, whereas $UCuAs_2$ structure is favored for an electron count of 24 or higher. With a three-dimensional model one actually reaches exactly the same conclusion.

Both U–Co and U–C distances are nearly same in the two structures. The U–Co bond is 2.97 Å in the $UCuAs_2$ structure and 2.93 Å in the $UCoC_2$ structure; the average U–C separations are 2.46 and 2.52 Å, respectively. With similar coordination environments and similar bond distances, the uranium atoms are expected to behave similarly in the two systems, and in fact they do. We have performed a series of calculations employing a full 3D model, including U atoms. The results resemble greatly those obtained in a two-dimensional approach. Again, the $UCoC_2$ structure reaches a maximum stabilization over the $UCuAs_2$ structure for an electron count of 20. The preference switches to the latter for electron counts over 23.

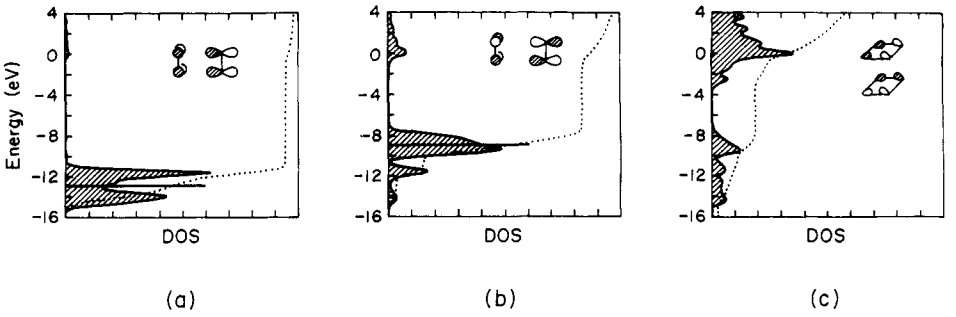

Figure 22. Density of states curves of CoC_2 2D lattice in $UCoC_2$ structure: (a) projected C_2 π contributions, (b) π^* orbitals, and (c) the e set of the cobalt "hollow" orbitals. Dotted lines are integrations, and molecular C_2 π and π^* orbital energies are indicated with sticks.

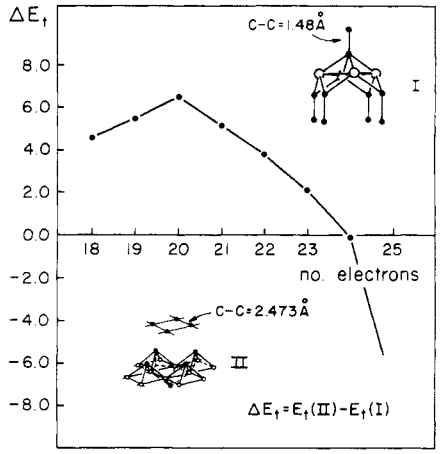

Figure 23. Average total energy change vs electron count. The curve is $\Delta E_t = E_t(II) - E_t(I)$, where I is the 2D CoC_2 in the $UCoC_2$ type structure and II, CoC_2 in the $UCuAs_2$ type structure.

The effect of uranium atoms on the C–C bond length is similar to that in the UC_2 structure. Interactions of their d orbitals with C_2 π and π^* levels lead to a ~75% filling of π states and a ~30% filling of π^* states. Compared to $UCoC_2$, the filling of π and π^* in $ScCoC_2$ is ~90% and ~15%, respectively, corresponding to a considerably shorter C–C bond of length 1.26 Å.

Fermi energies are calculated for $UCoC_2$ structure with several electron counts. They are indicated in Figure 24 along with the total density of states. It appears that compounds with 19, 21, and 22 electrons should be metallic, whereas no definitive answer can be given for an electron count of 20.

An interesting feature about ZrCuSiAs may be pointed out here. We have mentioned earlier that this structure belongs to the $UCuAs_2$ type, but with the As atoms in the 2a positions replaced by Si. One might ask why silicon atoms take up the 2a site instead of going to 2c positions. A charge distribution argument[92] may provide an explanation for this. The argument goes as follows: for a parent structure with nonequivalent sites, different electron densities are usually observed. Upon substitution, the more electronegative substituents will preferentially enter the sites of greater electron density.[93] Plotted in Figure 25 is the curve of electron density difference between 2a and 2c versus electron count for a parent structure. It is clear from this figure that the electron density is higher

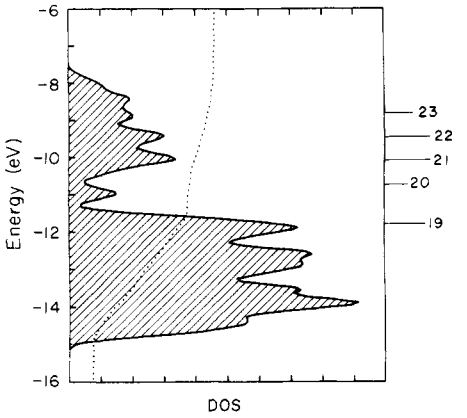

Figure 24. Total density of state projection for $UCoC_2$. Fermi energies are calculated for 19–23 electrons, respectively, and they are indicated with horizontal sticks at right of the plot.

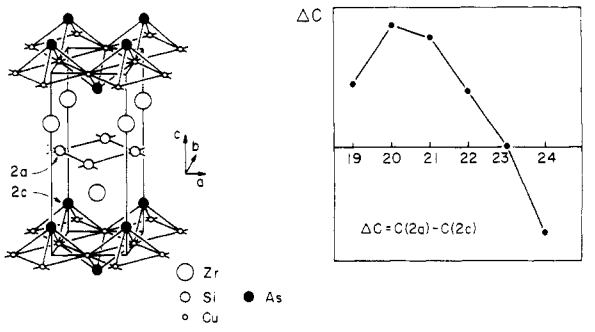

Figure 25. Electron density difference (Δc) between the two nonequivalent sites 2a and 2c in the $UCuAs_2$ parent structure versus number of electrons in the system.

in 2a for electron counts between 19 and 22. For systems with 23 electrons, 2a and 2c are approximately equal in electron density. 2c becomes more charged with compounds of 24 electrons or more. Since Si atoms are less electronegative than As and since ZrCuAsSi is a 24-electron species, it is not surprising to have silicon atoms occupying the 2a sites of lower electron density for that particular electron count.

An interesting question arises concerning the possibility of forming $ThCr_2Si_2$ type carbides. We have seen how this could be accomplished by inserting a transition-metal square lattice into the $UCoC_2$ structure in **22**. With a composition of 67% carbon, CaC_2 type compounds are the metal carbides richest in carbon. Adding one layer of metal, the carbon concentration in the $UCoC_2$ structures is reduced to 50%. Is it possible to proceed one step further, by inserting another metal layer, to form a carbide of the $ThCr_2Si_2$ type, in which the carbon percentage is reduced even further, to 40%? According to Jeitschko and

(92) (a) Burdett, J. K.; Lee, S.; Mclarnan, J. J. *J. Am. Chem. Soc.* **1985**, *107*, 3083. Burdett, J. K. *Prog. Solid State Chem.* **1984**, *15*, 173. (b) Chen, M. M. L.; Hoffmann, R. *J. Am. Chem. Soc.* **1976**, *98*, 1647. Hoffmann, R.; Howell, J. M.; Muetterties, E. L. *J. Am. Chem. Soc.* **1972**, *94*, 3047. (c) Gimarc, B. M. *J. Am. Chem. Soc.* **1983**, *105*, 1979.

(93) Li, J.; Hoffmann, R. *J. Phys. Chem.* **1988**, *92*, 887.

Table III. Atomic Parameters Used in the Calculations

orbital		H_{ii}, eV	ζ_1	ζ_2	c_1[a]	c_2[a]
U	7s	-5.51	1.91			
	7p	-5.51	1.91			
	6d	-5.12	2.58	1.21	0.7608	0.4126
Gd	6s	-7.67	2.14			
	6p	-5.01	2.08			
	5d	-8.21	3.78	1.38	0.7765	0.4587
Co	4s	-9.21	2.00			
	4p	-5.29	2.00			
	3d	-13.18	5.55	2.10	0.5680	0.6060
C	2s	-21.40	1.62			
	2p	-11.40	1.62			
Ca	4s	-7.00	1.20			
	4p	-4.00	1.20			

[a] Double ζ expansion coefficients of the orbitals.

co-workers, silicide analogues of such carbides are unlikely to be synthesized, because of the high coordination number (8 if there is no short C-C contact as in $ThCr_2Si_2$) around small carbon atoms.[18] They propose an alternative structure, a $ThCr_2Si_2$ type carbide with singly bonded carbon pairs, which may be particularly favorable for large, electropositive divalent metals. To see how the two structures differ electronically, we have performed a series of calculations using the two models described below: (I) a carbide of $ThCr_2Si_2$ type with carbon-carbon bonds of 1.50 Å and M-C separation of 2.47 Å and (II) a $ThCr_2Si_2$ metal-carbon structure with eight-coordinated carbon atoms, where the M-C bond is taken the same as in $UCoC_2$ and the C-C distance is a long 2.5 Å. Calculated total average energies for electron counts of 22-32 are listed in Table II. It seems that structure II continues to be preferred for lower electron counts. Such a preference is lost only for counts of 29 or more electrons in which case structure I becomes more favorable. Since one of the two carbon atoms in the 2c positions of a $UCoC_2$ structure is already 8-coordinated to uranium and cobalt, it seems not too unreasonable to think of configuration II as a candidate for carbides of RT_2C_2 composition by making the other carbon also eight-coordinated upon addition of a transition-metal square lattice to the $UCoC_2$.

Acknowledgment. This work is supported by the National Science Foundation through Research Grant CHE 8406119. J.L. would like to thank Marja Zonnevylle for some helpful suggestions. We are grateful to Jane Jorgensen and Elisabeth Fields for the drawings.

Appendix

An extended Hückel tight-binding approach is employed throughout this paper. Atomic parameters used in the calculations were taken from previous work[94] and are tabulated in Table III. Geometrical data for the UC_2, CaC_2, $DyCoC_2$, and $UCoC_2$ structure were obtained from reported X-ray crystallographic experimental results. Gd parameters were used for the Dy atoms. Several k-point sets were used in calculations of average properties. These were chosen according to the Pack and Monkhorst method[95a] as well as to the Ramirez and Böhm method.[95b]

(94) (a) Ortiz, J. V.; Hoffmann, R. *Inorg. Chem.* **1985**, *24*, 2095. Tatsumi, K.; Nakamura, A. *J. Am. Chem. Soc.* **1987**, *109*, 3195. (b) 68. (c) Summerville, R. H.; Hoffmann, R. *J. Am. Chem. Soc.* **1976**, *98*, 7240. (d) 69(a). (e) Zheng, C.; Hoffmann, R. *J. Am. Chem. Soc.* **1986**, *108*, 3078.

(95) (a) Pack, J. D.; Monkhorst, H. J. *Phys. Rev.* **1977**, *B16*, 1748. (b) Ramirez, R.; Böhm, M. C. *Int. Quantum Chem.* **1986**, *30*, 391.

Angularly Resolved Second Harmonic Generation Study of the Air-Formed Oxide on Iron

M. W. Schauer, M. J. Pellin, and D. M. Gruen*

Materials Science and Chemistry Divisions, Argonne National Laboratory, Argonne, Illinois 60439

Received August 8, 1988

By variance of the angle of incidence and input polarization, it is possible to obtain structural information about the oxide layer that forms on iron surfaces from angularly resolved second harmonic generation (AR-SHG) experiments. The AR-SHG experiments on air-oxidized (110) iron single-crystal surfaces reveal the presence of both 2-fold and 3-fold symmetric species at the metal/oxide interface. These patterns are fit to an extension of existing theory, and the 3-fold symmetric oxide is found to be tilted by about 5° from the Fe (110) plane. The 2-fold symmetric structure is aligned with the Fe (110) surface, and the SHG intensity contains both surface and bulk contributions.

Introduction

Structural information about the oxides that form on iron surfaces is crucial to the understanding of corrosion and passivation. The understanding of these phenomena has motivated innumerable studies since the discovery of the passive oxide layer on iron.[1] Much has been learned about the possible composition of the passive film that forms on iron and other metals, yet despite extensive study, the chemical and structural details of this very important system remain largely a mystery.

One of the unique capabilities of second harmonic generation (SHG) as a surface analytical tool is the ability to probe a solid-solid interface below the surface of a material. The dipolar contribution to the induced polarization in the medium that gives rise to the SHG signal is necessarily zero in bulk, isotropic material. Therefore, the major contribution to the signal in an SHG experiment arises near an interface, where the bulk symmetry is broken.

The tensorial nature of the second-order nonlinear susceptibility that governs SHG can be used to obtain structural information about an interface. The symmetry

(1) *Passivity of Metals*; Frankenthal, R. P., Kruger, J., Eds.; The Electrochemical Society: Princeton, NJ, 1978.

0897-4756/89/2801-0101$01.50/0